

Eruptive history and $^{40}\text{Ar}/^{39}\text{Ar}$ geochronology of the Milos volcanic field, Greece

Red texts represent the comments and corrections from Jocelyn McPhie (JM) and Peter Abbott (PA).

Xiaolong Zhou¹, Klaudia Kuiper¹, Jan Wijbrans¹, Katharina Boehm¹, Pieter Vroon¹

¹Department of Earth Sciences, VU University Amsterdam, De Boelelaan 1085, 1081 HV Amsterdam, The Netherlands.

Correspondence to: Xiaolong Zhou (z.x.l.zhou@vu.nl)

Abstract. High-resolution geochronology is essential ~~to determine~~^{for determining} the growth-rate of volcanoes, which is one of the key factors ~~to establish~~^{for establishing} the periodicity of ~~explosive~~ volcanic eruptions. However, there are less high-resolution eruptive histories ($>10^6$ years) determined for long-lived submarine arc volcanic complexes than for subaerial complexes, since ~~the~~ submarine volcanoes are far more difficult to observe than subaerial ones. In this study, high-resolution geochronology and major element data are presented for Milos Volcanic Field (VF) in the South Aegean Volcanic Arc, Greece.

The Milos VF has been active for over 3 ~~Myrs~~^{Ma}, and the first two million years of its eruptive history occurred in a submarine setting that has ~~been~~ emerged above sea level ~~nowadays~~. The long submarine volcanic history of the Milos VF makes it an excellent natural laboratory to study the growth-rate of a long-lived submarine arc volcanic complex. This study reports twenty-one new high-precision $^{40}\text{Ar}/^{39}\text{Ar}$ ages and major element compositions for eleven volcanic units of the Milos VF. This allows us to divide the Milos volcanic history into at least three periods of different ~~long-term~~^{long-term} volumetric volcanic output rate (Q_e). Period I (~~submarine~~, $\sim 3.3\text{-}2.1$ ~~1.336~~ Ma) and III (~~subaerial~~, 1.48 Ma-present) have low Q_e of $0.9 \pm 0.5 \times 10^{-5} \text{ km}^3 \cdot \text{yr}^{-1}$ and $0.25 \pm 0.05 \times 10^{-5} \text{ km}^3 \cdot \text{yr}^{-1}$, respectively. Period II (~~submarine~~, 2.1 ~~1.336~~ - 1.48 Ma) has a 3-12 times higher Q_e of $3.0 \pm 1.7 \times 10^{-5} \text{ km}^3 \cdot \text{yr}^{-1}$. The Q_e of the Milos VF is 2-3 orders of magnitude lower than the average for rhyolitic systems and continental arcs. ~~Most of the effusive eruptions of Period II are probably derived from magma chambers in the upper crust, whereas the more pumiceous units of Period I and III are probably related to lower crustal hot zone.~~

1 Introduction

Short-term eruptive histories and compositional variations of lavas and pyroclastic deposits of many arc volcanic fields are well established. However, high-resolution eruptive histories that extend back $> 10^5\text{-}10^6$ years have been determined only for a handful of long-lived subaerial arc volcanic complexes. Some examples are: Mount Adams (Hildreth and Lanphere, 1994), Tatará-San Pedro (Singer et al., 1997), Santorini (Druitt et al., 1999), Montserrat (Cole et al., 2002), Mount Baker (Hildreth et al., 2003a), Katmai (Hildreth et al., 2003b), and Ceboruco-San Pedro (Frey et al., 2004). In order to establish the growth rate of volcanic complexes and to disentangle the processes which are responsible for the eruption, fractionation, storage and transport of magmas over time, comprehensive geological studies are required. These include detailed field mapping, sampling, high-resolution geochronology and geochemical analysis. Based on these integrated studies, the ~~growth~~-rate of volcanoes can be determined to establish the periodicity of effusive and explosive volcanism.

The Milos Volcanic Field (VF) is a long-lived volcanic complex which has been active for over 3 ~~Myrs~~^{Ma}. The Milos VF erupted for a significant part of its life below sea level, similar to the other well studied volcanic structures in the eastern Mediterranean (Fytikas et al., 1986; Stewart and McPhie, 2006). The eruptive history of the Milos VF has been examined with a broad range of ~~the~~ chronostratigraphic techniques such as K-Ar, U-Pb, fission track, ^{14}C and biostratigraphy (e.g. Angelier et al., 1977, Fytikas et al., 1976, 1986, Traineau and Dalabakis, 1989, Matsuda et al., 1999, Stewart and McPhie, 2006, Van Hinsbergen et al., 2004 and Calvo et al., 2012). However, most of the published ages have been measured using the less precise K-Ar or fission track methods, and modern, high precision $^{40}\text{Ar}/^{39}\text{Ar}$ ages for the Milos VF have not been published so far. In this study, (1) we provide high-precision $^{40}\text{Ar}/^{39}\text{Ar}$ geochronology of key volcanic units of the Milos VF and (2) refine the

Commented [JM1]: should say which periods were submarine and which were subaerial because you say the submarine history is what makes Milos important

Commented [JM2]: magma chamber locations are outside the scope of the data presented; this topic should be omitted

40 stratigraphic framework of the Milos VF with the new high-precision $^{40}\text{Ar}/^{39}\text{Ar}$ ages and major element composition. (3) We
41 also quantify and constrain the compositional and volumetric temporal evolution of volcanic products of the Milos VF.

42 1.1 Geological setting

43 The Milos VF is part of the South Aegean Volcanic Arc (SAVA), an arc which was formed in the eastern Mediterranean by
44 subduction of the African plate beneath the Aegean microplate (Figure 1, Nicholls, 1971; Spakman et al., 1988; Duermeijer et
45 al., 2000; Pe-Piper and Piper, 2007; Rontogianni et al., 2011). The present-day Benioff zone is located approximately 90 km
46 underneath the Milos VF (Hayes et al., 2018). The upper plate is influenced by extensional tectonics (e.g. McKenzie, 1978;
47 Pe-Piper and Piper, 2013), which is evident on the island of Milos as horst and graben structures (Figure 2).

48 The Milos VF is exposed on the islands of the Milos archipelago: Milos, Antimilos, Kimolos and Polyegos. The focus of this
49 study is Milos with which has a surface area of 151 km² for the main island. The geology and volcanology of Milos have been
50 extensively studied in the last 100 years. The first geological map was produced by Sonder (1924). This work was extended
51 by Fytikas et al. (1976) and Angelier et al. (1977) and the subsequent publications by of Fytikas (Fytikas, (1989); and Fytikas
52 et al., (1986) and Fytikas (1989). Interpretations based on volcanic facies of the complete stratigraphy were made by Stewart
53 and McPhie (Stewart and McPhie, 2003, 2006). More detailed studies of single volcanic centres (e.g. Bombarda volcano and
54 Fyriplaka complex) were published by Campos Venuti and Rossi (1996) and Rinaldi et al. (2003). Milos has also been
55 extensively studied for its epithermal gold mineralization, that has been summarized by Alfieris et al. (2013). Milos was known
56 during the Neolithic period for its export of high quality obsidian. Today the main export product is kaolinite, that is mined
57 from hydrothermally altered felsic volcanic units in the centre of the island (e.g. Alfieris et al., 2013).

58 The geology of Milos can be divided into four main units: (1) metamorphic basement, (2) Neogene sedimentary rocks, (3)
59 volcanic sequences and (4) the alluvial cover. The metamorphic basement crops out at the southwest, south and southeast of
60 Milos (Figure 3) and is also found as lithic blocks in many volcanic units. The metamorphic rocks include lawsonite-free
61 jadeite eclogite, lawsonite eclogite, glaucophane schist, quartz-muscovite-chlorite and chlorite-amphibole schist (Fytikas et
62 al., 1976, 1986; Grasmann et al., 2018; Kornprobst et al., 1979). The exposed units belong to the Cycladic Blueschist Unit
63 (Lower Cycladic nappe), whereas eclogite pebbles in the phreatic eruption products (called green lahar by unit e.g. Fytikas,
64 1977) are derived from the Upper Cycladic Nappe (Grasmann et al., 2018).

65 On top of this metamorphic basement Neogene fossiliferous marine sedimentary rocks were deposited (e.g. Van Hinsbergen
66 et al. 2004). This sedimentary sequence can be divided into a lower unit A and upper unit B that is unconformably overlain
67 by volcanoclastic sediments (Van Hinsbergen et al., 2004). Unit A is 80 m thick and consists of fluvial-lacustrine, brackish
68 and shallow marine conglomerate, sandstone, dolomite and limestone. Unit B is 25-60 m thick and consists of a sandstone
69 overlain by a succession of alternating marls and sapropels, suggesting a deeper marine setting (Van Hinsbergen et al., 2004).
70 Five volcanic ash layers that contain biotite are found in this Neogene sedimentary rock sequence either suggesting that
71 volcanic eruptions in small volume already occurred in the Milos area, or that these ash layers are derived from larger eruptions
72 of volcanic centres further away from Milos (van Hinsbergen et al., 2004). Age determinations by bio-magneto- and cyclo-
73 stratigraphy suggested that deposition of Unit A started at approximately 5 Ma, and that Milos subsided 900 m in 0.6 million
74 years (Van Hinsbergen et al. 2004) due to extension. This subsidence happened ca 1.0-1.5 Ma before the onset of the main
75 phase of Pliocene- recent volcanism on Milos.

76 The Pliocene-recent volcanic sequence of Milos has been subdivided into different units by Angelier et al. (1977) and Fytikas
77 et al. (1986). In addition, Stewart and McPhie (2006) provided a detailed facies analysis of the different volcanic units. The
78 subdivision by Angelier et al. (1977) is not constrained well due to their limited amount of age data. The subdivision of volcanic
79 units by Fytikas et al. (1986) and facies descriptions of Stewart and McPhie (2006) are summarized below. It is important to
80 note that according to Stewart and McPhie (2006), the five volcanic cycles described by Fytikas et al. (1986) are difficult to
81 match with existing age data and the continuous progression in volcanic construction (Fig. 4). For example, the first phase of

Commented [JM3]: should explain what this unit is;
should have upper case

Commented [PA4]: You switch between Myrs and Ma,
should this not be consistent throughout the manuscript?

82 Fytikas et al. (1986), the Basal Pyroclastic Series, contains the large pumice cone-crypto dome volcanoes according to Stewart
83 and McPhie (2006). Two of these pumice-cone crypto dome volcanoes are much younger and intercalated between the
84 Complex of Domes and Lava Flows (CDLF) of Fytikas et al. (1986).

85 The first volcanic unit deposited in the Milos area is the Basal Pyroclastic Series (BPS) (Fytikas et al., 1986) or submarine
86 felsic cryptodome-pumice cone volcanoes (Stewart and McPhie, 2006, Figure 2-4). This unit consist of thickly bedded pumice
87 breccia with a rhyolitic-dacitic composition. These rhyolites-dacites are aphyric or contain quartz-feldspar±biotite phenocrysts.
88 Graded sandstone and bioturbated and fossil rich (in-situ bivalve shells) mudstone are intercalated, indicating a marine
89 environment and a water depth of several hundreds of meters (e.g. Stewart, 2003; Stewart and McPhie, 2006), whereas later
90 degassed magmas with a similar composition intruded as sills and cryptodomes. The BPS has been strongly affected by
91 hydrothermal fluids, especially the proximal deposits (e.g. Kiliass et al., 2001).

92 The second volcanic unit was named the Complex of Domes and Lava Flows (CDLF, Fytikas et al., 1986) and the volcanic
93 facies of this unit ~~is~~ ~~are~~ described as the submarine dacitic and andesitic domes by Stewart and McPhie (2006). This phase of
94 effusive submarine volcanism was predominantly andesitic/dacitic in composition and produced microcrystalline rocks with
95 phenocrysts of pyroxene, amphibole, biotite and plagioclase. The eruption centres were mainly located along NNE faults and
96 formed up to 300 m thick deposits extending over areas of 2.5 to 10 km² around the eruption centres. In the north-eastern part
97 of Milos, an andesitic scoria cone provided scoria lapilli and bombs to deeper water settings. Sandstone intercalated in the
98 CDLF contains both igneous and metamorphic minerals suggesting input from the basement. Rounded pebbles of rhyolite and
99 dacite indicate that some of the volcanic deposits were above sea level, or in very shallow, near shore environments (e.g.
100 Stewart and McPhie, 2006).

101 The third volcanic unit is called the Pyroclastic Series and Lava Domes (PSLD) by Fytikas et al. (1986) and belongs to
102 submarine-to-subaerial dacitic and andesitic lava domes of Stewart and McPhie (2006). This highly variable group is
103 dominated by rhyolitic, dacitic and andesitic lavas, domes, pyroclastic deposits and felsic pumiceous sediments (Stewart and
104 McPhie, 2006). Thickness varies between 50-200 m, and the deposits are located in the eastern and northern parts of Milos
105 (Figure 2 and 3). The initial pyroclastic layers were subaqueously deposited and the extrusion of a dome resulted in deposition
106 of talus around the margins by mass flow. On top of the dome sand- and siltstone with fossils (Ostrea fossil assemblage) and
107 traction-current structures suggest that the top of the dome was above wave base. The youngest deposits of this unit are dacitic
108 and andesitic lavas and domes. These domes generated subaerial block-and-ash flow and surge deposits. Paleosols within these
109 deposits are a clear indicator that some areas were above sea level. The last unit of the PSLD is represented by large subaerial
110 rhyolitic lava that contain quartz and biotite phenocrysts and is found near Halepa in the south-central part of Milos.

111 The fourth unit consists of the subaerially constructed rhyolitic Complexes of Trachilas and Fyriplaka (CTF) (Fytikas et al.,
112 1986), which Stewart and McPhie (2006) interpreted as subaerial rhyolitic lava-pumice cones. These two volcanic complexes
113 are built from rhyolitic pumice deposits and lavas that contain quartz and biotite phenocrysts (10-20 modal %). The deposits
114 have a maximum thickness of 120 m and decrease to several meters thickness in the distal parts. Basement-derived schist is
115 found as lithic clasts (Fytikas et al., 1986). In addition, the Kalamos rhyolitic lava dome, that outcrops on the southern coast
116 of Milos, produced a lava that spread westwards to the Fyriplaka beach (Figure 2). This lava belongs to this fourth phase and
117 is probably derived from an older volcano and not the Fyriplaka complex (Campos Venuti and Rossi, 1996).

118 The fifth volcanic unit comprises deposits from phreatic activity, especially in the northern part of the Zefiria Graben and near
119 Agia Kiriaki (Figure 2 of Stewart and McPhie, 2006). Many overlapping craters are surrounded by lithic breccias that are
120 composed of variably altered metamorphic basement clasts and volcanic clasts. This phreatic activity has continued into
121 historic times (Trainau and Dalabakis, 1989). Fytikas et al. (1986) ~~described-referred to~~ this unit as "green lahar", although
122 indicated that this deposit is not a lahar but the product of phreatic eruptions in the last 0.2 Ma.

Commented [JM5]: een lahar ee

123 **1.2 Previous geochronological studies**

124 Previous geochronological work is summarised in Table 1. Angelier et al. (1977) reported six K-Ar ages (0.95-2.50 Ma). These
125 ages were used in combination with field observations to divide the Milos volcanic succession into four units. However, the
126 samples from Fyriplaka, the fourth unit, were too young to be dated by Angelier et al. (1977). Fytikas et al. (1976, 1986)
127 published 16 K-Ar ages for Milos (0.09-3.50 Ma) including an age of 0.09-0.14 Ma for the Fyriplaka complex. Fytikas et al.
128 (1986) also obtained 3 K-Ar ages for Antimilos (0.32 ± 0.05 Ma), Kimolos (3.34 ± 0.06 Ma) and Polyegos (2.34 ± 0.17 Ma).
129 Trainau and Dalabakis (1989) dated the very young phreatic deposits by ^{14}C dating and found ages between 200 BC and 200
130 AD. Matsuda et al. (1999) published two K-Ar ages of 0.8 ± 0.1 (MI-1) and 1.2 ± 0.1 Ma (MI-4) for the Plakes dome that was
131 also studied by Fytikas et al. (1986). Bigazzi and Radi (1981) published two fission track ages of 1.54 ± 0.18 and 1.57 ± 0.15
132 Ma for obsidians of Bombarda-Adamas and Demenaghaki, respectively. Later fission track studies by Arias et al. (2006) (1.57
133 ± 0.12 and 1.60 ± 0.06 Ma) confirmed these ages. The fission track ages are younger than the K-Ar ages given by Angelier et
134 al. (1977; 1.84 ± 0.08 Ma for Demenaghaki) and Fytikas et al. (1986; 1.71 ± 0.05 Ma for Bombarda). In the most recent
135 geochronological study of the Milos VF, Stewart and McPhie (2006) published 4 SHRIMP U/Pb zircon ages: Triades dacite
136 facies (1.44 ± 0.08 and 2.18 ± 0.09 Ma), Kalogeros cryptodome (2.70 ± 0.04 Ma) and the Fylakopi Pumice Breccia ($2.66 \pm$
137 0.07 Ma). All uncertainties reported here are 1 standard deviation uncertainties as reported in the original publications, except
138 for the ^{14}C ages for which uncertainties were not specified.

139 **2 Methods**

140 **2.1 Mineral separation and sample preparation**

141 Samples were collected from all major volcanic units on Milos island as based on the studies of Fytikas et al. (1986), Stewart
142 and McPhie (2006) and our own observations in the field. Photos of the sample locations and thin sections can be found in the
143 supplementary material I. Approximately 2 kg of fresh juvenile pyroclastic pumice clasts or lava was sampled from each unit.
144 Samples were cut into ~ 5 cm³ cubes using a diamond saw to remove potentially altered surfaces and obtain the fresh interior
145 parts. These cubes were ultra-sonicated for 30 minutes in demi-water to remove dust and seawater and dried in an oven
146 overnight at 50 °C. Dry sample cubes were crushed in a steel jaw crusher, and this fraction was split into two portions of
147 roughly equal size. One of them was powdered in an agate shatter box and agate ball mill to a grain size of less than 2 μm for
148 the major-element analysis. The second fraction was sieved to obtain a grain size of 250-500 μm for $^{40}\text{Ar}/^{39}\text{Ar}$ dating.
149 Heavy liquids density separation techniques (Jl1st, 1973) were used to purify mineral separates (groundmass, biotite, amphibole)
150 required for the $^{40}\text{Ar}/^{39}\text{Ar}$ dating. Different densities of heavy liquids were used to obtain groundmass ($2700 \leq \rho \leq 3000$ kg.m⁻³),
151 biotite ($2900 \leq \rho \leq 3100$ kg.m⁻³) and/or amphibole ($\sim 3100 \leq \rho \leq 3200$ kg.m⁻³). A Franz Isodynamic Magnet-Magnetic
152 separator was used to remove the magnetic minerals from the non-magnetic minerals and groundmass. The samples for
153 $^{40}\text{Ar}/^{39}\text{Ar}$ analysis were purified by handpicking under a binocular optical microscope to select mineral grains without visible
154 alteration and inclusions.

155 **2.2 $^{40}\text{Ar}/^{39}\text{Ar}$ dating**

156 The mineral and groundmass samples were wrapped in either 6- or 9-mm aluminium foil and packed in 20 mm aluminium
157 cups, that were vertically stacked. Based on stratigraphy and previous geochronological constraints >1 Ma samples and the <1
158 Ma samples were irradiated for ~~respectively~~ 7 and 1 hours ~~respectively~~ in irradiation batches VU108 and VU110 in the
159 Cadmium-Lined in-Core Irradiation Tube (CLICIT) facility of the Oregon State University Training Research, Isotopes,
160 General Atomics (TRIGA) reactor. The neutron flux for all irradiations was monitored by standard bracketing using the
161 Drachenfels sanidine (DRA; 25.52 ± 0.08 Ma, modified from Wijbrans et al., 1995 and calibrated relative to Kuiper et al.,
162 2008) and Fish Canyon Tuff sanidine (FCs; 28.201 ± 0.023 Ma, Kuiper et al., 2008) with Min et al. (2000) decay constants.

Commented [JM6]: clarify - do you mean juvenile clasts such as pumice clasts from pyroclastic deposits? or do you mean lithified/welded pyroclastic

Commented [PA7]: Expand acronyms

163 In total 24 samples (8 groundmasses, 15 biotites and 2 amphiboles, for sample G15M0026 both biotite and amphibole were
164 analysed) were measured by either $^{40}\text{Ar}/^{39}\text{Ar}$ fusion and/or incremental heating techniques. For incremental heating
165 experiments 80-100 grains per sample were loaded into a 25-hole (surface per hole $\sim 36\text{ mm}^2$) copper tray together with single
166 grain standards in $\sim 12\text{ mm}^2$ holes. The tray was prebaked in vacuum (10^{-5} - 10^{-6} mbar) at $250\text{ }^\circ\text{C}$ overnight to remove
167 atmospheric argon and subsequently baked overnight at $120\text{ }^\circ\text{C}$ in the ultra-high vacuum sample chamber ($<5 \times 10^{-9}$ mbar) and
168 purification system connected to a Thermo Scientific Helix MC mass spectrometer.

169 Samples and standards were heated with a focused laser beam at 8 % power using a 50W CW CO_2 laser. The released gas was
170 cleaned by exposure to a cold trap cooled by a Lauda cooler at $-70\text{ }^\circ\text{C}$, a SAES NP10 at $400\text{ }^\circ\text{C}$, Ti sponge at $500\text{ }^\circ\text{C}$ and cold
171 SAES ST172 Fe-V-Zr sintered metal. The five isotopes of argon were measured simultaneously on five different collectors:
172 ^{40}Ar on the H2-Faraday, ^{39}Ar on the H1-Faraday or the H1-CDD, ^{38}Ar on the AX-CDD, ^{37}Ar on the L1-CDD and ^{36}Ar on the
173 L2-CDD for 15 cycles with 33 seconds integration time (CDD: compact discrete dynodes). The Faraday cups on H2 and H1
174 were equipped with $10^{13}\text{ }\Omega$ amplifiers. Procedural blanks were measured every 2 or 3 analyses in different sequences, and
175 air-shots were measured every 8-12 hours to correct the instrumental mass discrimination. Gain between different collectors
176 was monitored by measuring CO_2 on mass 44 in dynamic mode on all collectors. Gain was generally stable over periods of
177 weeks. Note, that because samples, standards and air calibration runs are measured during the same period, gain correction
178 does not substantially change the final age results. The raw mass spectrometer data output was converted by an in-house
179 designed Excel macro script to be compatible with the ArArCalc 2.5 data reduction software (Koppers, 2002). The $^{40}\text{Ar}/^{36}\text{Ar}$
180 atmospheric air value of 298.56 from Lee et al. (2006) is used in the calculations. The correction factors for neutron interference
181 reactions are $(2.64 \pm 0.02) \times 10^{-4}$ for $(^{36}\text{Ar}/^{37}\text{Ar})_{\text{ca}}$, $(6.73 \pm 0.04) \times 10^{-4}$ for $(^{39}\text{Ar}/^{37}\text{Ar})_{\text{ca}}$, $(1.21 \pm 0.003) \times 10^{-2}$ for $(^{38}\text{Ar}/^{39}\text{Ar})_{\text{K}}$
182 and $(8.6 \pm 0.7) \times 10^{-4}$ for $(^{40}\text{Ar}/^{39}\text{Ar})_{\text{K}}$. All uncertainties are quoted at the 1σ level and include all analytical errors (i.e. blank,
183 mass discrimination and neutron interference correction and analytical error in J-factor, the parameter associated with the
184 irradiation process).

185 A reliable plateau age is defined as experiments with at least 3 consecutive steps overlapping at 2-sigma, containing $>50\%$ of
186 the $^{39}\text{Ar}_{\text{K}}$, a Mean Square Weighted Deviate (MSWD) value <2.5 , and with an $^{40}\text{Ar}/^{36}\text{Ar}$ inverse isochron intercept that does
187 not deviate from atmospheric argon at 2-sigma. All the inverse isochron ages used the same steps as used in the weighted mean
188 ages, and all relevant analytical data for the age calculations following standard practices (Schaen et al., 2020) can be found
189 in the supplementary material II.

190 2.3 Whole-rock major element analysis by XRF

191 Major-element concentrations were measured by X-ray fluorescence spectroscopy (XRF) on a Panalytical AxiosMax. A
192 Panalytical Eagon2 was used to create 40mm fused glass beads of $\text{Li}_2\text{B}_4\text{O}_7/\text{LiBO}_2$ (65.5:33.5%, Johnson & Johnson
193 Spectroflux 110) with a 1:6 dilution sample-flux ratio that were molten at $1150\text{ }^\circ\text{C}$. Sample powders were ignited at $1000\text{ }^\circ\text{C}$
194 for 2 hours to determine loss on ignition (LOI) before being mixed with the $\text{Li}_2\text{B}_4\text{O}_7/\text{LiBO}_2$ flux. Interference corrected spectra
195 intensities were converted to oxide-concentrations against a calibration curve consisting of 30 international standards. The
196 precision, expressed as the coefficient of variation (CV), is better than 0.5%. The accuracy, as measured on the international
197 standards AGV-2, BHVO-2, BCR-2 and GSP-2 was better than 0.7% (1 RSD) (supplementary material III).

198 2.4 Rock textural analysis and Eruption volume calculations

199 The crystallinity and vesicularity were estimated with Image J software by scanning the thin section of each sample 4-6 times
200 to cover the entire area. For the crystallinity only the phenocrysts were considered, crystals smaller than $50\text{ }\mu\text{m}$ were included
201 in the groundmass. The estimations of crystallinity and vesicularity on the older samples ($>1.0\text{ Ma}$) of Milos VF are all from
202 lava and domes. The younger samples ($<1.0\text{ Ma}$) are from pumiceous pyroclastic units. The other old pumices of the Profitis
203 Ilias and Filakopi volcanoes are not included in this study due to the severe alteration that prevents the collection of reliable

Commented [PA8]: Use symbol

Commented [PA9]: Include units. Or if it is a ratio make that clearer

Commented [JM10]: how did you determine crystallinity of pumiceous samples? Did you correct for the volume occupied by vesicles?

Commented [JM11]: The data are therefore not representative and cannot be used to detect trends

204 geochemical and geochronological data on these samples. The mean value and standard deviation of the crystallinity and
205 vesicularity were also calculated.

206 The minimum and/or maximum eruption volume of each volcano during each eruption period is derived from the ranges of
207 thickness and surface areas that are reported in Campos and Rossi (1996) and Stewart and McPhie (2006). We converted these
208 volumes to Dense Rock Equivalent (DRE) based on the magma type of different deposits. This analysis only includes the
209 onshore deposits and results in a smaller estimate for larger pyroclastic volumes. The DRE volume is calculated using the
210 equation of (Croweller et al., 2012):

$$DRE (km^3) = \frac{tephra\ vol (km^3) \times tephra\ density (kg/m^3)}{magma\ density (kg/m^3)}$$

212 Tephra density is assumed to be 1000 kg/m³ (Croweller et al., 2012). Magma density varies depending on the magma type.
213 Here we used 2300 kg/m³ for rocks with a SiO₂ range of 65-77 wt.% and 2500 kg/m³ for all samples with SiO₂ < 65 wt.%
214 (Table 4 for major element composition). DRE corresponds to the unvesiculated erupted magma volume and DRE volumes
215 are converted to include vesicularity. Therefore, we did not convert the volume of some cryptodome and lavas from Profitis
216 Illias (G15M0017), Triades (G15M0021-24), Dhemenehaki (G15M0032B) and Halepa (G15M0013) to the DRE since they
217 contain less than 5% vesicles.

Commented [JM12]: Conversion to DRE volumes is required ONLY for non-welded pyroclastic deposits. You need to distinguish between the non-welded pyroclastic units and lavas/domes/welded pyroclastic units.

Commented [JM13]: this makes no sense. DRE converts vesicular to non-vesicular - why would you then convert DRE to include vesicularity?

218 3 Results

219 3.1 ⁴⁰Ar/³⁹Ar age results

220 In this section, we present our groundmass, biotite and amphibole ⁴⁰Ar/³⁹Ar results for eleven volcanic units of Milos. The
221 ⁴⁰Ar/³⁹Ar ages range from 0.06 to 4.10 Ma and cover most of the major volcanic units of Milos. Table 2 and 3 show the
222 ⁴⁰Ar/³⁹Ar results of incremental heating steps and single grain fusion analyses, respectively. Note that the Irr-ID column in
223 these two Tables represents the irradiation ID of the analytical experiment (e.g. VU108-, VU110-) and the top right superscripts
224 (G, B, A, O) in the sample IDs (e.g., G15M0029^G, G15M0021^B) refer to groundmass, biotite, amphibole and obsidian.

225 3.1.1 Groundmass ⁴⁰Ar/³⁹Ar plateau and/or isochron ages

226 All groundmass samples yielding ⁴⁰Ar/³⁹Ar plateau and isochron ages with more than 50% ³⁹Ar_K and less than 2.5 MSWD
227 included in their age spectrum are shown in Figure 4 and reported in Table 2. The ⁴⁰Ar/³⁶Ar isochron intercepts do not deviate
228 from atmospheric argon at the 2-sigma level, unless stated otherwise (Table 3). Sample G15M0016 was collected from a dyke
229 at Klefiko in the southwest of Milos (Figure 2). Three incremental heating experiments were performed on the groundmass
230 of this sample (Figure 5A). The first experiment (VU108-Z8a) produced a weighted mean age of 2.71 ± 0.02 Ma (MSWD
231 2.31; ³⁹Ar_K 79.6%; inverse isochron age 2.65 ± 0.10 Ma). The other two, VU108-Z8a_4 and VU108-Z8b_1, have plateau ages
232 of 2.61 ± 0.03 Ma (MSWD 0.93; ³⁹Ar_K 57.4%; inverse isochron age 2.69 ± 0.10 Ma) and 2.67 ± 0.01 Ma (MSWD 1.50; ³⁹Ar_K
233 65.57%; inverse isochron age 2.55 ± 0.05 Ma), respectively. The three experiments are remarkably similar. Although the
234 amount of radiogenic ⁴⁰Ar is low (<20%), a combined age of 2.66 ± 0.01 Ma is considered to be best estimate with a relatively
235 high MSWD value (2.51).

236 Two lava samples, G15M0019 and G15M0020, were collected from Kontaro in north-eastern Milos (Figure 2). Three replicate
237 incremental heating steps experiments of on groundmass from sample G15M0019 (VU108-Z6a_4; VU108-Z6a_5 and VU108-
238 Z6b_1, Figure 5B) were performed that are not reproducible. Their plateau ages range from 1.55 Ma to 1.62 Ma with relatively
239 high MSWD (3.8-4.5), 56-95% of the total ³⁹Ar_K, 34-53% of radiogenic ⁴⁰Ar, 0.88-1.02 of K/Ca and an atmospheric isochron
240 intercept of 297-315. We consider the isochron age from the last experiment (VU108-Z6b_1) as the only-reliable age (1.48 ±
241 0.02 Ma, MSWD 0.44) because of the-its MSWD value is the only one smaller than 2.5 least scatter in this experiment, and
242 therefore the best estimate for the eruption age. Three replicate incremental heating steps experiments of on groundmass from

Commented [PA14]: This doesn't make sense so please rephrase

243 sample G15M0020 (VU108-Z5a_5; VU108-Z5b_1 and VU108-Z5b_2, Figure 5C) were analysed. These experiments are
244 similar at the lower temperature heating steps. They produced statistically meaningful plateau ages ranging from 1.52-1.56 Ma
245 with 41-62% of the total $^{39}\text{Ar}_K$, 18-48% of radiogenic ^{40}Ar , 1.51-1.73 of K/Ca and an atmospheric isochron intercept of 295-
246 300. Their combined weighted mean age is 1.54 ± 0.01 Ma (MSWD 3.06; $^{39}\text{Ar}_K$ 57.32%) with 25.31% of $^{40}\text{Ar}^*$.
247 Sample G15M0032B (obsidian) was collected from a pumice cone volcano at Demeneghaki (Figure 2). One incremental
248 heating experiment ~~of on~~ this sample (VU108-Z18, Figure 5D) yielded a plateau age of 1.825 ± 0.002 Ma (MSWD 0.91; $^{39}\text{Ar}_K$
249 98.6%). The $^{40}\text{Ar}^*$ is 93.86%. The inverse isochron age is identical to the weighted mean plateau age 1.825 ± 0.002 Ma. The
250 age of 1.825 ± 0.002 Ma is considered the best estimate for the eruption age of the Demeneghaki obsidian.

251 3.1.2 Groundmass $^{40}\text{Ar}/^{39}\text{Ar}$ plateau and/or isochron ages (25-40% $^{39}\text{Ar}_K$ released)

252 The results shown in Figure 5 did not yield weighted mean plateau ~~ages~~ according to standard criteria including $^{39}\text{Ar}_K > 50\%$,
253 but still provide some useful age information. Sample G15M0017 was collected from a cryptodome of the Profitis Illias
254 volcano of southwestern Milos (Figure 2). Three replicate incremental heating experiments, VU108-Z7a, VU108-Z7a_4 and
255 VU108-Z7b_1, have been performed on this sample which resulted in disturbed age spectra (Figure 6A). The consecutive
256 lower temperature steps of all experiments define ages of < 2.5 Ma, which is much younger than the ages of the submarine
257 pyroclastic products of the lower series at Kleftiko and/or Profitis Illias (3.0-3.5 Ma, Fytikas et al., 1986 and Stewart and
258 McPhie, 2006). At the consecutive higher temperature heating steps, these experiments yielded 3.64 ± 0.08 Ma ($^{40}\text{Ar}/^{36}\text{Ar}$
259 293.87 ± 4.77 ; VU108-Z7a), 4.10 ± 0.06 Ma ($^{40}\text{Ar}/^{36}\text{Ar}$ 298.44 ± 15.51 ; VU108-Z7a_4) and 3.41 ± 0.05 Ma ($^{40}\text{Ar}/^{36}\text{Ar}$ 295.97
260 ± 7.34 ; VU108-Z7b_1). The total fusion and inverse isochron ages of the three experiments gave large ranges of 2.25-3.23 and
261 3.68-4.14 Ma, respectively, and none of these high temperature heating steps produced a statistical plateau (all MSWD > 2.0).

262 The amount of radiogenic ^{40}Ar of both ~~the~~ $^{40}\text{Ar}/^{39}\text{Ar}$ result from our sample and ~~the~~ K-Ar age data from previous studies
263 (Fytikas et al., 1986) is rather low ($< 15\%$) for a sample of this age based on our laboratory experience. Therefore, the estimated
264 age range for the oldest volcanic products of the Milos VF should be confirmed by other dating techniques.

265 Sample G15M0015 is also a cryptodome breccia from Profitis Illias (Figure 2). Two replicate incremental step heating
266 experiments were performed on the groundmass of this sample (VU108-Z9a and VU108-Z9b_1, Figure 6B). Experiment
267 VU108-Z9a groundmass shows a disturbed age spectrum ~~with and~~ ages ~~increasing-increase~~ from ~ 3 Ma in the initial heating
268 steps to ~ 3.2 Ma, followed by a decrease to ~ 3 Ma in the high temperature heating steps. The consecutive heating steps only
269 exist at the lower temperature steps yielding a "plateau" of 3.12 ± 0.02 Ma (MSWD 9.07). Due to the excess argon ($^{40}\text{Ar}/^{36}\text{Ar}$
270 304.19 ± 1.25 comprising 43.07% of the released $^{39}\text{Ar}_K$), the inverse isochron of 3.06 ± 0.02 Ma (MSWD 0.01) is more reliable
271 for this analysis. The inverse isochron age of the second groundmass (VU108-Z9b_1) is identical at 3.04 ± 0.02 Ma (MSWD
272 1.14; $^{39}\text{Ar}_K$ 27.00%) and $^{40}\text{Ar}/^{36}\text{Ar}$ of 293.83 ± 1.38 obtained at high temperature steps. The two experiments are remarkably
273 similar. Although the sample does not formally fulfil the definition of a plateau age comprising $> 50\%$ $^{39}\text{Ar}_K$ released, a
274 combined age of 3.06 ± 0.02 Ma (MSWD 1.14; $^{39}\text{Ar}_K$ 22.79%, $^{40}\text{Ar}^*$ 41.77%) most likely represents the eruption age. This
275 $^{40}\text{Ar}/^{36}\text{Ar}$ age is consistent with the K-Ar age from the same lithology of 3.08 ± 0.08 Ma (Fytikas et al. 1986).

276 Sample G15M0029 is an andesite collected from Korakia in the northeast of Milos (Figure 2). Two incremental heating
277 experiments (VU108-Z16a and VU108-Z16b_1, Figure 6C) were performed on this sample. The two experiments are
278 remarkably similar ~~with and show~~ a decreasing age from ~ 2.85 Ma at the lower temperature heating steps to 2.65 Ma at the
279 higher temperatures. The higher temperature heating steps of both experiments yielded weighted mean plateau ages of $2.67 \pm$
280 0.01 Ma (MSWD 0.96; $^{39}\text{Ar}_K$ 23.61%, $^{40}\text{Ar}^*$ 56.34%; inverse isochron age 2.68 ± 0.02 Ma) and 2.69 ± 0.01 Ma (MSWD 1.32;
281 $^{39}\text{Ar}_K$ 27.08%, $^{40}\text{Ar}^*$ 55.78%; inverse isochron age 2.67 ± 0.03 Ma). The isochron intercepts for both experiments are
282 atmospheric. The combined age of 2.68 ± 0.01 Ma should be considered with caution due to the rather low amount of released
283 ^{39}Ar (23-28%).

284 3.1.3 Single biotite grain $^{40}\text{Ar}/^{39}\text{Ar}$ fusion and/or isochron ages

285 Results of nine single fusion experiments are given in Figure 7. Nine or ten replicate single fusion experiments were conducted
286 on 5-10 grains biotite per fusion. Sample G15M0006 is from ~~a solid in situ~~ dacite with columnar joints from the Kalogeros
287 cryptodome in the northeast of Milos (VU108-Z11, Figure 7A). The sample shows a weighted mean age of 2.72 ± 0.01 Ma
288 ~~with for~~ 9 out of 10 total fusion experiments (MSWD 1.95; 9/10) with an average 47.9% of radiogenic ^{40}Ar . The inverse
289 isochron age is 2.62 ± 0.04 Ma (MSWD 0.99). Note that excess argon ($^{40}\text{Ar}/^{36}\text{Ar}$ 310.2 \pm 4.0) is present, hence the inverse
290 isochron age is younger compared to the weighted mean age. The isochron age of 2.62 ± 0.04 Ma is considered as the best
291 estimate for the emplacement age.

292 Sample G15M0025 was collected from the Mavros Kavos lava dome located in the west of Milos (Figure 2). The biotite of
293 this sample (VU108-Z2, Figure 7B) shows a weighted mean age of 2.36 ± 0.01 Ma (MSWD 0.70; 9/10; $^{40}\text{Ar}^*$ 37.60%, inverse
294 isochron age 2.34 ± 0.04 Ma) with an $^{40}\text{Ar}/^{36}\text{Ar}$ intercept of 300.6 ± 3.5 . The age of 2.36 ± 0.01 Ma is considered the best
295 eruption age estimate for this sample.

296 Sample G15M0023 and ~~24G15M0024~~ are from the Triades lava dome ~~of the~~ northeast of Milos (Figure 2). A mafic enclave
297 G15M0022 (host rock G15M0021) was collected from a lava near Cape Vani (Figure 2). The total fusion experiments of the
298 biotites show that their initial $^{40}\text{Ar}/^{36}\text{Ar}$ estimates overlap with air (296-300). The total fusion ages gave the best estimates for
299 their eruption ages of 2.10-2.13 Ma using 22 out of 31 fusions with a range of radiogenic ^{40}Ar between 30-36% (Figure 7B).

300 Sample G15M0013 is from the rhyolitic Halepa lava dome in the south of Milos (Figure 2). The total fusion experiment
301 (VU108-Z13, Figure 7C) on biotite of this sample produced a weighted mean age of 1.04 ± 0.01 Ma (MSWD 1.62; 9/10, $^{40}\text{Ar}^*$
302 26.3%; inverse isochron age 1.02 ± 0.04 Ma) with an initial $^{40}\text{Ar}/^{36}\text{Ar}$ estimate of 299.8 ± 4.1 . The best estimate for the
303 eruption age of the Halepa rhyolite is 1.04 ± 0.01 Ma.

304 Sample G15M0034 and ~~35-G15M0035~~ were collected from a lava dome located southeast of the Trachilas cone (Figure 2).
305 Nine total fusion experiments (VU108-Z21, Figure 7C) were performed on biotite of sample G15M0035 and yielded ~~the age~~
306 ~~of~~ 0.63 ± 0.02 Ma (MSWD 1.26; 6/9; $^{40}\text{Ar}^*$ 4.9%; inverse isochron age 0.77 ± 0.13 Ma). The atmospheric isochron intercept
307 overlaps with air at 2-sigma (296.4 ± 1.7). The 4.9% of radiogenic ^{40}Ar is so low that we should consider the age of $0.63 \pm$
308 0.02 Ma with caution. For biotite of sample G15M0034 (VU108-Z20, Figure 7C) one total fusion experiment produced a
309 weighted mean age of 0.51 ± 0.02 Ma (MSWD 0.95; 6/10; $^{40}\text{Ar}^*$ 3.5%; inverse isochron age 0.61 ± 0.08 Ma) with an
310 atmospheric isochron intercept. The age of 0.51 ± 0.02 Ma also needs to be considered as possibly suspect due to the low
311 amount of radiogenic ^{40}Ar .

312 Sample G15M0033 was collected from the Kalamos lava along the coast of the southwest of the Fyriplaka rhyolitic complex
313 (Figure 2). Biotite of this sample (VU108-Z19, Figure 7C) yielded 0.412 ± 0.004 Ma (MSWD 1.10; 8/10; inverse isochron
314 age 0.39 ± 0.02 Ma) with $\sim 22.2\%$ of radiogenic ^{40}Ar which is considered as the eruption age for the Kalamos lava.

315 3.1.4 Multiple biotite grain $^{40}\text{Ar}/^{39}\text{Ar}$ incremental heating plateau and/or isochron ages

316 Figure 8 displays the biotite $^{40}\text{Ar}/^{39}\text{Ar}$ ages measured by the incremental heating steps method. Sample G15M0021 is the host
317 lava of mafic enclave G15M0022. Twelve replicate total fusion experiments ~~ef on~~ its biotite (VU110-Z4, Table 3) produced
318 an age of 2.48 ± 0.04 Ma (MSWD 1.49; 4/12, $^{40}\text{Ar}^*$ 36.09%; inverse isochron age 3.44 ± 0.46 Ma). Although this suggests a
319 correct age, the large analytical error of each fusion (>0.3 Ma on average) and poor reproducibility (4/12) of this experiment
320 probably results in an unreliable age. Therefore, two more incremental heating experiments were performed on this sample
321 (VU110-Z4_2 and VU110-Z4_2b, Figure 8A), that gave an age of 1.97 ± 0.01 Ma (MSWD 1.66; $^{39}\text{Ar}_K$ 63.8%, $^{40}\text{Ar}^*$ 54.7%;
322 inverse isochron age 1.97 ± 0.03 Ma) and 2.01 ± 0.01 Ma (MSWD 6.76; $^{39}\text{Ar}_K$ 75.39%, $^{40}\text{Ar}^*$ 57.84%; inverse isochron age
323 2.04 ± 0.05 Ma), respectively. The scatter in the latter is too high to define a reliable plateau age and the first incremental
324 heating experiment is considered as the best estimate of the eruption age of this sample.

325 Sample G15M0007 was collected from the rhyolitic Trachilas complex in the north of Milos (Figure 2). Twenty-two total
326 fusion (VU110-Z12, Table 3) and two incremental heating experiments (VU110-Z12a and 12b, Figure 8B) were performed
327 on biotite of this sample. The total fusion experiments did not result in a reliable age due to the large errors of single steps (\pm
328 0.19 Ma on average) and the rather low amount of radiogenic ^{40}Ar (9.1%). On the other hand, the first incremental heating
329 experiment produced a plateau age of 0.30 ± 0.01 Ma (MSWD 4.61; $^{39}\text{Ar}_K$ 56.60%; inverse isochron age 0.28 ± 0.05 Ma)
330 including 14.51% of radiogenic ^{40}Ar . The second incremental heating experiment yielded a plateau of 0.317 ± 0.004 Ma
331 (MSWD 1.29; $^{39}\text{Ar}_K$ 74.05%; inverse isochron age 0.31 ± 0.03 Ma) with a higher amount of radiogenic ^{40}Ar (18.30%). The
332 isochron intercepts of both incremental heating experiments are atmospheric. The second experiment is the best estimate for
333 the eruption age, since it contained the largest amount of radiogenic ^{40}Ar and has a better reproducibility of single heating
334 steps.

335 Three pumice clasts (G15M0008-9 and G15M0012) were sampled from different layers of the Fyriplaka complex (Figure 2).
336 The first incremental step heating experiment ef-on biotite from sample G15M0009 (VU110-Z23a, Figure 8C) gave negative
337 ages at the lower temperature heating steps. Four consecutive higher temperature heating steps seem to define a “plateau” of
338 0.11 ± 0.02 Ma (MSWD 1.37) only using 18.33% of the total $^{39}\text{Ar}_K$ with 1.65% of radiogenic ^{40}Ar . The second experiment
339 (VU110-Z23b) also yielded a “plateau” of 0.11 ± 0.03 Ma (MSWD 6.77) at higher temperature heating steps including 41.05%
340 of the total $^{39}\text{Ar}_K$ and 3.13% of radiogenic ^{40}Ar . The significantly larger error of the isochron age may be due to the clustering
341 of data close to zero on the y-axis. The two experiments (VU110-Z23a and Z23b) are comparable. The combined age of 0.11
342 ± 0.02 (MSWD 3.5) is consistent with the age of 0.09-0.14 Ma from Fytikas et al. (1986). Although only 29.50% of the released
343 $^{39}\text{Ar}_K$ was used for this sample, we believe this age is the eruption age of this layer in the Fyriplaka complex.

344 For biotite of sample G15M0012 both incremental step heating experiments are comparable. Both of them yielded plateau
345 ages of 0.05 ± 0.01 Ma (VU110-Z24a; MSWD 3.09; $^{39}\text{Ar}_K$ 38.89%, $^{40}\text{Ar}^*$ 2.89%; inverse isochron age 0.14 ± 0.03 Ma) and
346 0.09 ± 0.02 Ma (VU110-Z24b; MSWD 8.16; $^{39}\text{Ar}_K$ 48.04%, $^{40}\text{Ar}^*$ 4.59%; inverse isochron age 0.09 ± 0.05 Ma) at higher
347 temperature heating steps (Figure 8C). The clustering of data points of experiment VU110-Z24a could result in the lower
348 initial estimate of $^{40}\text{Ar}/^{36}\text{Ar}$ (285.98 ± 4.76). However, the combined age of 0.07 ± 0.01 Ma, using 43.53% of the total $^{39}\text{Ar}_K$
349 with an atmospheric isochron intercept (295.67 ± 7.39), could be the representative age of eruption.

350 Biotite of sample G15M0008 did not result in a reliable plateau in the first incremental step heating experiment (VU110-Z22a,
351 Figure 8C) but shows a very disturbed age spectrum. The second experiment (VU110-Z22b) yielded 0.062 ± 0.003 Ma (MSWD
352 0.91) using 71.81% of the total $^{39}\text{Ar}_K$ with 2.69% of radiogenic ^{40}Ar as the best estimate of the eruption age.

353 3.1.5 Multiple amphibole grain $^{40}\text{Ar}/^{39}\text{Ar}$ multi-grain incremental heating plateau and/or isochron ages

354 There are only two amphibole samples that yielded $^{40}\text{Ar}/^{36}\text{Ar}$ plateau and/or isochron ages (Figure 9A and B). Sample
355 G15M0004 was collected from the pyroclastic series of Adamas from the PSLD (Fytikas et al., 1986), to the north of Bombarda
356 (Figure 2). Two replicate heating experiments of G15M0004 amphibole (VU108-Z10_1 and VU108-Z10_2) were performed
357 yielding 2.99 ± 0.11 Ma (MSWD 1.00; $^{39}\text{Ar}_K$ 87.31%, $^{40}\text{Ar}^*$ 16.36%; inverse isochron age 7.89 ± 2.46 Ma) and 2.86 ± 0.09
358 Ma (MSWD 1.50; $^{39}\text{Ar}_K$ 86.18%, $^{40}\text{Ar}^*$ 17.58%; inverse isochron age 0.70 ± 0.29 Ma). The variable atmospheric isochron
359 intercept of both experiments ($^{40}\text{Ar}/^{36}\text{Ar}$ 202.39 ± 48.47 and 348.91 ± 27.33) is due to clustering of the data points. Note that
360 also the amount of radiogenic ^{40}Ar is rather low (~17%). The two experiments are remarkably similar. A combined inverse
361 isochron age of 1.95 ± 0.45 Ma (MSWD 1.17; $^{40}\text{Ar}/^{36}\text{Ar}$ 319.51 ± 14.70) is considered the best estimate, but ideally this age
362 should be checked by other techniques.

363 Sample G15M0026 is from the same location as sample G15M0025, which gives us the opportunity to compare the biotite age
364 with the amphibole age. One total fusion experiment ef-on biotite (VU108-Z1b) yielded a weighted mean age of 2.35 ± 0.01
365 Ma (MSWD 1.36; $^{40}\text{Ar}^*$ 38.6%). The atmospheric isochron intercept is low ($^{40}\text{Ar}/^{36}\text{Ar}$ 292.01 ± 2.92), the inverse isochron
366 age of 2.42 ± 0.04 Ma (MSWD 0.93) is considered the best result from the biotite. Two incremental heating experiments for

367 amphibole (VU108-Z1b_1 and VU108-Z1b_2) gave plateau ages of 2.67-2.70 Ma which are much higher values than the
368 biotite inverse isochron ages (2.28-2.31 Ma). This result could be caused by the high $^{40}\text{Ar}/^{36}\text{Ar}$ isochron intercepts (>320) with
369 large uncertainties of ~29. Therefore, on the basis of the remarkable similarity of the two experiments, the combined inverse
370 isochron age of 2.31 ± 0.28 Ma (MSWD 0.93, $^{39}\text{Ar}_K$ 71.36%, $^{40}\text{Ar}^*$ 34.97%) is considered as the best estimate from amphibole
371 which overlaps with the biotite age of 2.42 ± 0.03 Ma. This biotite age of 2.42 ± 0.03 Ma is considered to the best approximation
372 of the eruption age.

373 3.2 Major element results

374 Major-element results are given in Table 4. The major element compositions range from 54 to 78 wt.% SiO_2 (basaltic-andesite-
375 rhyolite to dacite-rhyolite, see Figure 10A). The most felsic samples ($\text{SiO}_2 > 75$ wt.%) belong to the Fyriplaka and Trachilas
376 complexes. Our data overlap with those of previous studies and display a similar range in SiO_2 - K_2O (Francalanci and Zellmer,
377 2019 and reference therein). The samples of Polyegos are similar to the Fyriplaka and Trachilas complexes, whereas the older
378 Milos samples overlap with Kimolos and Antimilos (Fytikas et al., 1986, Francalanci et al., 2007).
379 Although some samples of Antimilos are tholeiitic, all of the Milos volcanic units belong to the calc-alkaline and medium to
380 high-K series (Figure 10B). A mafic inclusion, sample G15M0022, has high K_2O (6%), similar to sample G15M0021 (7.2
381 wt.%). Both of them were collected from the Vani Cape area (Fig. 2). The SiO_2 wt.% versus our $^{40}\text{Ar}/^{39}\text{Ar}$ ages diagram (Figure
382 11A) shows that there is a tendency of the volcanic units to become more felsic over time. In the diagram with $\text{K}_2\text{O}/\text{SiO}_2$
383 versus age there is no significant change (Figure 11C).

384 3.3 Variations of rock texture and eruption volume with ages

385 Figure 11D and E show the variations of crystallinity and vesicularity of the studied samples versus the $^{40}\text{Ar}/^{39}\text{Ar}$ ages. There
386 is a lack of geochemical and petrological data offor the pumice deposit of the Profitis Iliias (>3.0 Ma). The other old pumiceous
387 pyroclastic unit, Filakopi (~2.66 Ma) volcano, has low crystallinity (<10%) and high vesicularity (10-100%) based on the data
388 of Stewart (2003). Before 1.48 Ma, the crystallinity of the Milos volcanic units is relatively high (10-40%) and vesicularity
389 varies between 1-10%. After 1.48 Ma, the lava unit of the Halepa dome and the young pumiceous unit of Trachilas and
390 Fyriplaka complexes (<1.0 Ma) have low crystallinity (<10%), and the high vesicularity (10-100%). [The volcanic complex
391 of Milos was largely (~85% by volume) constructed before ~1.48 Ma (Figure 11A). During Between 1.48 Ma present, only a
392 small volume (~15%) of rhyolitic magma was added from different eruption vents.

393 Figure 11a shows the cumulative volcanic output volume of the Milos VF over time. This diagram shows that the Milos VF
394 can be separated into three periods: Periods I (~3.3-2.13 Ma) and III (1.48-0.00 Ma) are characterised by low volcanic output
395 volumes, whereas Period II (2.13-1.48 Ma) shows a rapid increase in volcanic output volume. Period I and II are build up in
396 submarine settings, whereas Period III is in a subaerial setting. The Milos VF was largely (~85% by volume) constructed in
397 submarine before ~1.48 Ma (Period I and II) (Figure 11A). During Period III (1.48 Ma-present), only a small volume (~15%)
398 of rhyolitic magma was added from different eruption vents. See the details of Period I-III in section 4.3.2.

399 4 Discussion

400 In this section, our $^{40}\text{Ar}/^{39}\text{Ar}$ results are compared with previously published geochronological data, and subsequently used to
401 refine the stratigraphy of the Milos VF. In the last part, we will discuss the temporal variations in major elements and the
402 volumetric volcanic output rate of the Milos VF.

Commented [JM15]: I think this should be entirely omitted; your data are so biased to young units that it is impossible to detect reliable trends.

Commented [JM16]: should integrate information on submarine versus subaerial setting data here - was the 85% before ~1.48 Ma all submarine?

403 4.1 Comparison with the previous geochronological studies on the Milos VF

404 K-Ar ages may show undesirable and unresolvable scatter due to various problems: (1) in accurate determination of radiogenic
405 argon due to either incorporation of excess argon or incomplete degassing of argon during the experiments; (2) inclusion of
406 cumulate or wall rock phenocrysts in bulk analyses; (3) disturbance of a variety of geological processes such as slow cooling,
407 thermal reheating; (4) unrecognized heterogeneities due to separate measurements of potassium and argon content by different
408 methods; (5) requirement of relatively large quantities (milligrams) of pure sample (e.g. Lee, 2015). In addition to these
409 methodological issues, in the case of Milos we observe that hydrothermal alteration caused substantial kaolinitisation, in
410 particular the felsic volcanic samples, that most likely has affected the K-Ar systematics. Some of these issues are also valid
411 for the $^{40}\text{Ar}/^{39}\text{Ar}$ method, however, the K-Ar method does not allow testing if ages are compromised.

412 $^{40}\text{Ar}/^{39}\text{Ar}$ ages only need isotopes of argon to be measured from a single aliquot of sample with the same equipment that can
413 eliminate some of the problems with sample inhomogeneity. Furthermore, step heating and multiple single fusion experiments
414 can shed light on sample inhomogeneity due to partial alteration effects. The high sensitivity of modern noble gas mass
415 spectrometers for $^{40}\text{Ar}/^{39}\text{Ar}$ measurements results in very small sample amounts needed for analysis, that can yield more
416 information on the thermal or alteration histories than larger samples. Moreover, other argon isotopes (^{36}Ar , ^{37}Ar and ^{38}Ar) can
417 be used to infer some information about the chemical compositions (i.e. Ca and Cl) of samples. A high-resolution laser
418 incremental heating method of $^{40}\text{Ar}/^{39}\text{Ar}$ dating allows us to resolve the admixture of phenocryst-hosted inherited ^{40}Ar in the
419 final temperature steps of the incremental step heating experiments. More than half of our $^{40}\text{Ar}/^{39}\text{Ar}$ ages derived for this study
420 are based on this method. All incremental step heating experiments are reproducible, except for the sample G15M0017 which
421 gave the oldest age. The total fusion experiments of this study gave at least five times smaller analytical uncertainty (1SE on
422 average ≤ 0.01 Ma) than the previous studies using conventional K-Ar (Angelier et al., 1977; Fytikas et al., 1976, 1986; Matsuda
423 et al., 1999) and SHRIMP U/Pb zircon methods (Stewart and McPhie, 2006). Fission track dating on obsidians of the Milos
424 VF produced two ages (Bigazzi and Radi, 1981; Arias et al., 2006) which seems to overlap with the K-Ar and $^{40}\text{Ar}/^{39}\text{Ar}$ ages,
425 but with larger uncertainty. U/Pb zircon ages could indicate the timing of zircon formation at high temperature (>1000 °C) in
426 magma chambers significantly prior to volcanic eruption (e.g. Flowers et al., 2005). On the other hand, the lower closure
427 temperature of K-rich minerals (<700 °C) makes the K-Ar and $^{40}\text{Ar}/^{39}\text{Ar}$ ages better suited to determine the timing of extrusion
428 of volcanic products (e.g. Grove and Harrison, 1996; Cassata and Renne, 2013).

429 The MSWD value, as a measure of the scatter of the individual step ages, is based on the error enveloping around the data
430 point. The decrease in error will automatically cause an increase in MSWD (e.g. York, 1968; Wendt and Carl, 1991). The
431 MSWD values reported in this study are relatively high. In part this is caused by the fact that modern multi-collector mass
432 spectrometers used for $^{40}\text{Ar}/^{39}\text{Ar}$ dating can measure the isotope ratios very precisely, which in turn would increase the MSWD.
433 It will be more valuable and challenging to find a plateau or isochron age which meets the MSWD criteria (<2.5) by modern
434 multi-collector $^{40}\text{Ar}/^{39}\text{Ar}$ dating than by K-Ar or $^{40}\text{Ar}/^{39}\text{Ar}$ dating using a single detector instrument (e.g. Mark et al., 2009).

435 Potential drawbacks of the $^{40}\text{Ar}/^{39}\text{Ar}$ method are its dependence on neutron irradiation causing the production of interfering
436 argon isotopes that need to be corrected for. The uncertainty in ages of standards that are required to quantify the neutron flux
437 also needs to be incorporated in the final ages as are uncertainties related to decay constants (supplementary material II).
438 Finally, recoil can occur during irradiation. Minerals such as biotite can be prone to recoil, yielding slightly older ages (e.g.
439 Hora et al., 2010).

440 Figure 13-12 compares previous published K-Ar, U/Pb zircon and fission track ages from the same volcanic units with the new
441 $^{40}\text{Ar}/^{39}\text{Ar}$ data of this study. In general, there is a good agreement, however, six ages out of twenty-three differ significantly
442 from previous studies ~~that and~~ will be discussed below.

443 The obsidian fission track ages (Bigazzi and Radi, 1981; Arias et al., 2006) for the Dhemenehaki volcano are 0.25 My younger
444 than the K-Ar ages (1.84 Ma, Angelier et al., 1977) and the $^{40}\text{Ar}/^{39}\text{Ar}$ age of this study (1.825 Ma, G15M0032B). The good
445 agreement between the K-Ar and $^{40}\text{Ar}/^{39}\text{Ar}$ ages suggests that the fission track ages record another, lower temperature event,

Commented [JM17]: This review should be greatly shortened and shifted to the Introduction. Review that does not relate to the data presented (only the technique) should not be in the Discussion.

446 than the K-Ar and $^{40}\text{Ar}/^{39}\text{Ar}$ ages. In addition, the larger uncertainty of fission track ages (>0.05 Ma) also overlaps with the
447 $^{40}\text{Ar}/^{39}\text{Ar}$ age at 2-sigma. We assume that the $^{40}\text{Ar}/^{39}\text{Ar}$ age is the correct extrusion age for the obsidian of the Dhemenehaki
448 volcano.

449 Angelier et al. (1977) reported one dacite sample in the northwest of Milos with an age of 1.71 Ma (Angelier_3, location 3 on
450 Figure 3 of Angelier et al., 1977). Argon loss could result in these ages (Angelier_3-5 in Figure 4312) being younger than our
451 $^{40}\text{Ar}/^{39}\text{Ar}$ groundmass ages of 1.97 ± 0.01 Ma (dacite sample G15M0021 and -22).

452 The amphibole of sample G15M0004 of the Adamas dacitic lava dome, located ~1 km north of rhyolitic Bombarda volcano,
453 gave an inverse isochron age of $1.95 \text{ Ma} \pm 0.45 \text{ Ma}$. This age overlaps with the K-Ar age for the Adamas lava dome of $2.03 \pm$
454 0.06 Ma (dacite M 66) of Fytikas et al. (1986). The large analytical uncertainty of our sample G15M0004 is caused by a
455 combination of low $^{40}\text{Ar}^*$ yields and clustering of data points that define the inverse isochron showing excess argon was
456 identified by the $^{40}\text{Ar}/^{39}\text{Ar}$ method ($^{40}\text{Ar}/^{36}\text{Ar}$ 319.51 \pm 14.70), whereas the presence of excess argon cannot be tested by the
457 K-Ar technique, implying that the Fytikas et al. (1986) might be slightly old.

458 The Korakia andesite has an age of $1.59 \pm 0.25 \text{ Ma}$ (M 103, Fytikas et al., 1986) and was deposited in a submarine-subaerial
459 environment on top of the Sarakiniko Formation that was dated based on paleomagnetic polarity in combination with a K-Ar
460 age (1.80-1.85 Ma, Stewart and McPhie, 2003 and reference therein). The much older $^{40}\text{Ar}/^{39}\text{Ar}$ groundmass age (2.68 ± 0.01
461 Ma) of Korakia andesite sample G15M0029 is unreliable and it could indicate the emplacement age of the Kalogeros
462 cryptodome ($2.70 \pm 0.04 \text{ Ma}$, Stewart and McPhie, 2006) or represents a geological meaningless age with only 23-27% of the
463 total ^{39}Ar released in the "plateau". In this case, the K-Ar age of $1.59 \pm 0.25 \text{ Ma}$ is considered as the likely eruption age for the
464 Korakia andesite although its argon loss or excess Ar component is unknown.

465 We obtained $^{40}\text{Ar}/^{39}\text{Ar}$ ages of 3.41-4.10 Ma and $3.06 \pm 0.02 \text{ Ma}$, respectively, from the groundmasses of dacite samples
466 G15M0017 and G15M0015 in the southwest of Milos (Figure 2 and 44B13B). Both of these samples are derived from the
467 coherent dacite facies of the rhyolitic Profitis Illias volcano based on the Figure 11 of Stewart and McPhie (2006). Sample
468 G15M0015 yielded much higher radiogenic ^{40}Ar (41.77%) than that of sample G15M0017 ($<10\%$ of $^{40}\text{Ar}^*$), and the rhyolite
469 sample M 164 from Fytikas et al. (1986) (23.5% of $^{40}\text{Ar}^*$) gave an estimate the eruptive age of $3.08 \pm 0.08 \text{ Ma}$ to the Profitis
470 Illias volcano which is much younger than that given by our sample G15M0017 (Figure 4312). Therefore, we considered our
471 $^{40}\text{Ar}/^{39}\text{Ar}$ ages of $3.06 \pm 0.02 \text{ Ma}$ ~~is-as~~ the best estimate of the emplacement age of the coherent dacite facies of Profitis Illias
472 volcano.

473 A basaltic andesite dyke near Klefiko on the south-western coast of Milos has a K-Ar age of $3.50 \pm 0.14 \text{ Ma}$ which only gave
474 13.9% of $^{40}\text{Ar}^*$ (Fytikas et al. 1986). This age is significantly older than the eruptive ages of Profitis Illias volcano which ~~they~~
475 ~~the dyke intruded~~ (Stewart, 2003). Although containing relatively low $^{40}\text{Ar}^*$ (16.87%), our $^{40}\text{Ar}/^{39}\text{Ar}$ age of $2.66 \pm 0.01 \text{ Ma}$
476 with 67.27% of $^{40}\text{Ar}^*$ from the groundmass of basaltic andesitic sample G15M0016 of the dyke near Klefiko is probably an
477 accurate intrusion age.

478 4.2 The published ages of other volcanic units

479 Unfortunately, we were not able to date all key volcanic units of the Milos VF. ~~This has~~ForThis was due to three reasons: (1)
480 we did not collect samples from all units; (2) some of the collected samples were not fresh enough after inspection of thin
481 sections; and (3) some of the $^{40}\text{Ar}/^{39}\text{Ar}$ data indicates that the K-Ar decay system was disturbed. Therefore, we include
482 published age information to establish a complete high-resolution geochronology for the Milos VF.

483 The published volcanic units that we include are the Profitis Illias volcano ($3.08 \pm 0.08 \text{ Ma}$ with 23.5 (%), Fytikas et al., 1986),
484 the Mavro Vouni lava dome ($2.50 \pm 0.09 \text{ Ma}$ with 55.2 $^{40}\text{Ar}^*$ (%), Anglier et al., 1977) in the south-western part of Milos, the
485 Bombarda volcano ($1.71 \pm 0.05 \text{ Ma}$ with 24.3 $^{40}\text{Ar}^*$ (%), Fytikas et al., 1986), the Plakes volcano ($0.97 \pm 0.06 \text{ Ma}$ with 10.2
486 $^{40}\text{Ar}^*$ (%), Fytikas et al., 1986, and 0.8-1.2 Ma with 5.4-11.9 $^{40}\text{Ar}^*$ (%) Matsuda et al. 1999). Scoria deposits that Stewart and
487 McPhie (2006) attributed to an andesitic scoria cone between Milos and Kimolos were produced in submarine, and maybe

488 occasionally above sea level. No age data for this deposit has been published so far. However, the stratigraphic position of this
489 scoria deposit is between MIL 365 (2.66 Ma, Stewart and McPhie, 2006) and M103 (1.59 Ma, Fytikas et al., 1986), which is
490 shown in Figure 10 of Stewart and McPhie (2006). Therefore, this scoria cone was likely active in the north-eastern part of the
491 Milos VF between 2.6 and 1.6 Ma.

492 Fytikas et al. (1986) also analysed a pumice coming from the Sarakiniko deposits eastward of Adamas (1.85 ± 0.10 Ma with
493 $13.6 \text{ }^{40}\text{Ar}^*$ (%), Fytikas et al., 1986) (Fig. 2). This unit is a reworked pyroclastic sediment of the Adamas lava dome (Rinaldi
494 and Venuti, 2003). Therefore, the K-Ar age from the Sarakiniko unit is not considered as an eruption age in this study. We did
495 not sample the neighbouring islands of the Milos VF and also did not attempt to date the products of the recent phase of
496 phreatic activity that from which Traineau and Dalabakis (1989) obtained ^{14}C ages of 200 BC and 200 AD.

497 4.3 Implications for the stratigraphy of the Milos VF

498 4.3.1. Start of volcanism in the Milos VF:

499 Figures 13 and 14 summarize our stratigraphic interpretation of the Milos VF based on our new $^{40}\text{Ar}/^{39}\text{Ar}$ ages in
500 combination with previously published stratigraphic, biostratigraphic, fission track, ^{14}C , K-Ar and U-Pb ages age data. We did
501 not consider the Matsuda et al. (1999) data as the fission-track ages seem to be offset to other dating techniques ages obtained
502 from the same deposits (see section 4.1 above). The exact start of volcanism in the Milos VF is still unclear since these older
503 deposits are strongly hydrothermally altered. Van Hinsbergen et al. (2004) reported five ash layers in the Pliocene sedimentary
504 rocks of southern Milos, ranging between 4.5-3.7 Ma in age, based on biostratigraphy, magnetostratigraphy and astronomical
505 dating. In a slightly wider circle around Milos island, the 6.943 ± 0.005 Ma a1-tephra event recorded in several locations on
506 nearby Crete (Rivera et al., 2011), shows that explosive volcanism along the Aegean arc, possibly on Milos, already occurred
507 during the Messinian. These ash beds cannot be traced to currently exposed centres in the Milos VF and could conceivably be
508 related to volcanic centres further north (Antiparos and Patmos), which were active during this time interval (Vougioukalakis
509 et al., 2019).

510 Biostratigraphy shows that the youngest layer with dateable fossils (bio-event, the last common occurrence of
511 Sphenolithus spp., Van Hinsbergen et al., 2004) in the Neogene sedimentary rocks is 3.61 Ma old (GTS2020, Raffi et al.,
512 2020). The diatomite Unit II from Calvo et al. (2012) on top of the oldest volcanoclastic deposit from the north-eastern coast
513 of Milos is constrained within 2.83-3.19 Ma. These data suggest that the oldest products must be older than 2.83 Ma and
514 younger than 3.61 Ma. Our oldest $^{40}\text{Ar}/^{39}\text{Ar}$ ages of this study displayed a wide range of 3.41-4.10 Ma that are probably not
515 correct due to alteration of the samples. Alteration might induce Ar loss and that would imply that the age is even older than
516 3.4-4.1 Ma. The age of 3.50 ± 0.14 Ma given by Fytikas et al. (1986) for an andesitic pillow lava or dyke has been discussed
517 above and probably belongs to a series of basaltic andesite intrusions in the younger dacitic-rhyolitic deposits of Profitis Ilias
518 (~ 3.08 Ma, Fytikas et al., 1986), and therefore the 3.5 Ma age is probably not correct (e.g. Stewart, 2003). Fytikas et al. (1986)
519 measured one sample from Kimolos (Figure 2 and 3) with an age of 3.34 Ma. Furthermore, Ferrara et al. (1980) reported an
520 age of 3.15 Ma for a lithic clast derived from the Petalia intrusion in the Kastro volcanoclastics of Polyegos. If we assume that
521 this reported age is a cooling age, volcanism in the Milos VF must have started before 3.15 Ma. Although age constraints for
522 the start of volcanism on Milos both from the Neogene sedimentary rocks and the dated volcanic samples are poor, the evidence
523 at this stage would suggest that volcanism in the Milos VF started ~ 3.3 Ma ago.

524 4.3.2. Periods with different volumetric output:

525 The volume estimates of the Milos VF are hampered by limited exposure of several volcanic units and unknown age
526 relationships. Therefore, not all units can be attributed to a certain volcano. Furthermore, we also do not know how much the
527 volcanic material was products were lost through transport by air, sea currents and erosion. Given the large errors on these
528 estimates, we only considered the rough difference in density between extruded magma and the calculated DRE values. The
529

Commented [JM18]: ??

530 ~~volumetric contributions of the islands Polygos, Kimolos and Antimilos are not considered here.~~ Therefore, the discussion
531 here only provides a first order estimate of the onshore extruded magma volume. Taken into account all these limitations, our
532 age data and the volume estimates by Stewart and McPhie (2006) ~~likely~~ indicate at least three periods of different ~~long~~
533 ~~term/long-term~~ volumetric volcanic output rates (Q_e) ~~throughout the Milos volcanic activity of from~~ ~3.3 ~~to~~ 0.0 Ma. We define
534 a “Period” as a time interval where the Q_e is significantly different from ~~the average output rate~~ (Q_e average = 1.0×10^{-5} km³·yr⁻¹
535 ~~) of the Milos VF over the last 3.3 Ma.~~ Figure 11 shows that the Q_e can be subdivided into two slow-~~growth~~ periods (I and
536 III) and one period (II) during which the Q_e was significantly larger.

Commented [JM19]: already said this at 48-49

Formatted: Subscript

Commented [JM20]: give what this average rate is

537 The lower boundary of Period I is based on our estimate of the ~~first-oldest~~ volcanic units of Milos at ~3.3 Ma. These
538 ~~first-oldest~~ units ~~have been were~~ deposited in the ~~SW-southwest~~ of Milos between ~3.3 and 3.08 Ma (~~see above~~) ~~that were~~
539 ~~mapped as large pumiceous deposits of and include~~ the ~~basal pyroclastic series by BPS~~ of Fytikas et al. (1986) and the felsic
540 pumice cone/crypto dome facies ~~by of~~ Stewart and McPhie (2006). These deposits have a minimum thickness of 120 m. The
541 estimates of the DRE volume and Q_e of these earliest volcanic deposits are hampered by the lack of precise age information,
542 the high degree of alteration and structural complexities. Therefore, we only calculated the Q_e of Period I ~~since from~~ 3.08 Ma
543 ~~from for~~ which the eruption products are mainly dacitic-rhyolitic in composition (Table 5, Fig 11), and the first products that
544 can be ~~reliable-reliably~~ dated are cryptodomes (3.06 Ma, sample G15M0015) and ~~dikes-dykes~~ (2.66 Ma, sample G15M0016)
545 into the ~~older basal pyroclastic series BPS~~ of Fytikas et al. (1986) or the units of Profitis Ilias volcano of Stewart and McPhie
546 (2006, 3.08 Ma) in the ~~SW-southwest~~ of Milos. ~~This/These cryptodomes and dykes was were~~ followed by the formation of the
547 submarine Fylakopi pumice cone volcano at 2.66 Ma (Stewart and McPhie, 2006) and Kalogeros cryptodome at 2.62 Ma
548 (sample G15M0006) in the north-eastern part of Milos. These two pumice cone volcanoes contributed 3-11 km³ DRE in
549 volume to the Milos VF. The last two volcanic activities of Period I occurred in the ~~SW-southwest~~ (Mavro Vauni, 2.50 Ma,
550 Angelier et al., 1977) and west of Milos (Mavros Kavos, 2.36 Ma, this study), respectively, which produced two high-aspect-
551 ratio andesitic-dacitic lava domes with a total volume of 1-3 km³ DRE (Stewart and McPhie, 2006). During ~~the submarine~~
552 Period I, which lasted ~ ~~1.2 Myr/Ma~~, the estimated Q_e is $0.9 \pm 0.5 \times 10^{-5}$ km³·yr⁻¹.

Commented [JM21]: this what?

Commented [JM22]: say whether this period was submarine or subaerial

553 The change from Period I to II is based on the sharp increase in Q_e ~~of Figure 11~~ at 2.13 Ma (~~Fig. 11~~). During this
554 period the Q_e ($3.0 \pm 1.7 \times 10^{-5}$ km³·yr⁻¹) increased by a factor of ~3 compared to ~~the~~ Period I and III. Period II ~~starts-began~~
555 with the ~~submarine~~ extrusions of the dacitic-rhyolitic Triades lava dome in the north-west and dacitic Adamas lava dome in
556 the north-east of Milos and ~~is-was~~ followed by the rhyolitic Dhemenehaki pumice cone/cryptodome and the Bombarda
557 volcano in the north-east of Milos. For the Bombarda centre a large age range is reported in the literature (1.71-2.15 Ma, Fig.
558 13B). We ~~were-did~~ not successfully ~~to~~ date samples from the Bombarda centre, but Rinaldi and Campos Venuti (2003) reported
559 that an age of 1.71 Ma is the best approximation based on other stratigraphic information. For the Dhemenehaki centre, we
560 obtained a ⁴⁰Ar/³⁹Ar age of 1.825 ± 0.002 Ma from obsidian. The Triades, Adamas, Dhemenehaki and Bombarda centres all
561 developed in ~~a~~ submarine settings, as the intercalated sediments from the northern coast of Milos show (Calvo et al., 2012; ~~see~~
562 Fig. 14). The last two volcanic expressions in Period II consists of two submarine-to-subaerial lava dome extrusions, Kantaro
563 (1.59 Ma, Fytikas et al., 1987) and Korakia (1.48 Ma, this study) in the north-west and north-east of Milos, respectively. The
564 products of these two centres are andesitic-dacitic in composition. All volcanic centres of Period II produced 8-30 km³ DRE
565 in volume for the Milos VF. ~~Each dome of Period II has a massive core and flow-banded rind surrounded by an in-situ~~
566 ~~autobreccia zone (Stewart and McPhie, 2006).~~

567 Period III ~~starts-began~~ with a time interval of 0.4 Ma with no eruptions and has a very low Q_e of $0.25 \pm 0.05 \times 10^{-5}$
568 km³·yr⁻¹. The boundary between Period II and III can be placed at the last eruption of Period II, at the start of the first eruption
569 in the low output interval, or halfway in between. The difference between those options is not significant, given the large
570 uncertainties of the volume estimates (Fig. 12), and therefore we have decided to start Period III directly after the last eruption
571 of the high Q_e of Period II. The composition of nearly all Period III volcanic products is rhyolitic, an exception is the dacitic
572 Plakes lava dome (Fig. 12). The Plakes lava dome is probably the last volcano erupting at ~0.97 Ma (Fytikas et al., 1987) in a

573 submarine environment in the north of Milos, whereas the other lava dome in Period III, Halepa, produced rhyolitic lavas in a
574 subaerial setting in the south (Stewart and McPhie, 2006). The Halepa and Plakes domes contributed 1-3 km³ DRE in volume
575 to the Milos VF and were followed by a 0.3 Ma interval with no or limited volcanic eruptions. Two subaerial pumice cone
576 volcanoes with biotite bearing rhyolites were constructed during the last 0.6 Ma-, the Trachilias and Fyriplaka complexes. The
577 Trachilias complex was active for approximately 300 kyr (0.63-0.32 Ma) in the northern part of Milos. The evolution of this
578 complex ~~starts began~~ with phreatic eruptions which became less explosive over time (Fytikas et al., 1986). During the last
579 eruption (0.317 ± 0.004 Ma) of the Trachilias complex rhyolitic pumices filled up the crater area and did breach the northern
580 tuff cone walls. The Trachilias complex only added a small volume (1-2 km³ DRE) ~~of material~~ to the Milos VF. The Kalamos
581 lava dome was also extruded in the south of Milos (Fig. 2) contemporaneously with the Trachilias complex.

582 The youngest volcanic activity of Milos (0.11 Ma-present), is characterized by subaerial eruptions of biotite phric
583 rhyolite from the Fyriplaka complex in the south of Milos, and was studied in detail by Campos Venuti and Rossi (1996). This
584 complex is constructed on a paleosol that developed in a phreatic deposit ("Green Lahar", Fytikas et al., 1986) or lies directly
585 on the metamorphic basement. Campos Venuti and Rossi (1996) indicated that the stratigraphic order is: Fyriplaka and Gheraki
586 tuff rings, Fyriplaka lava flow, ~~composed~~ tuff cone of Tsigrado-Provatas. ~~The tuff ring of Fyriplaka was divided into three~~
587 ~~members, with on top the deposits of the Tsigrado tuff cone.~~ The total estimated volume of volcanic material is 0.18 km³ DRE.
588 The boundary between the Fyriplaka and Tsigrado tuff cones is characterized by a marked erosive unconformity. The
589 composition of these young volcanic products is very constant (Fig. 10-11), ~~this was also~~ noted by Fytikas et al. (1986) and
590 Campos Venuti and Rossi (1996). The products from Fyriplaka and Tsigrado cones are covered ~~with by~~ a paleosol rich in
591 archaeological remains and a phreatic deposit consisting largely of greenschist metamorphic fragments. According to Campos
592 Venuti and Rossi (1996), the Fyriplaka cone was quickly built by phreatic and phreatomagmatic eruptions, as there are no
593 paleosols observed between the different units. However, our data do suggest a large range in ages between 0.11 and 0.06 Ma.
594 Fytikas et al. (1986) also reported a range between 0.14 and 0.09 Ma. These ages are inconsistent with the "Green Lahar" age
595 of 27 kyrs (Principe et al., 2002), suggesting that the "Green Lahar" deposit consists of many different phreatic eruption layers
596 that were formed during a time interval of more than 0.4 Ma, as the Kalamos lava is underlain by a green phreatic eruption
597 breccia (Campos Venuti and Rossi 1996). We, therefore, conclude that phreatic eruptions occurred for more than 400 kyr,
598 ~~predominantly~~ in the eastern part of Milos until historical times (200 BC – 200 AD, Traineau and Dalabakis, 1989).

599 4.3.3. Temporal evolution of the magma flux and composition plumbing system of the Milos VF.

600 Figure 11 shows ~~several of the~~ temporal petrographic and major-element variations during the evolution of the Milos VF. ~~The~~
601 ~~chemistry of the magmas did not change significantly between the three different periods, for example the K₂O/SiO₂ ratio is~~
602 ~~constant (0.05 ± 0.02) with one exception, sample G15M0021 collected near Cape Vani which is altered by hydrothermal~~
603 ~~processes (e.g. Alfieris et al. 2013).~~ The volcanic units of Period III are dominantly rhyolitic in composition, whereas during
604 Period I and II the compositions of volcanic units range between basaltic-andesite to rhyolite. ~~However, the K₂O/SiO₂ ratio is~~
605 ~~constant (0.05 ± 0.02) over the 3.3 Ma evolution of the Milos VF, with one exception, sample G15M0021 collected near Cape~~
606 ~~Vani which is altered by hydrothermal processes (e.g. Alfieris et al. 2013). ~~The crystallinity of the volcanic products is low~~~~
607 ~~(<10 vol.%) during Period III because most of these products are pumiceous. Although there is also a large number of~~
608 ~~pumiceous units of low crystallinity produced by Profitis Ilias and Fylakopi volcanoes during Period I (Stewart and McPhie,~~
609 ~~2006), the crystallinity of the other products of Period I and most of Period II units are much higher (20-40 vol.%) than that of~~
610 ~~Period III. In addition, we observed that the volcanic products of Period II have the lowest vesicularity (<10 vol.%), compared~~
611 ~~to the highly variable vesicularity of Period I (1-50 vol.%) and the high value for Period III (10-100 vol.%). These observations~~
612 ~~are consistent with the type of volcanic structures. Period I and III contain large explosive pumice cone volcanoes, whereas~~
613 ~~Period II is dominated by effusive dome extrusions. The difference in volcanic structures is not observed in the SiO₂ content~~
614 ~~and the K₂O/SiO₂ ratio of the volcanic products. ~~The~~ extrusion of crystal-rich, outgassed and thus viscous residual magmas in~~
615

Commented [JM23]: not in reference list

Commented [JM24]: This statement (595) contradicts 597-598 - clearly SiO₂ varied widely

Commented [JM25]: this sentence makes no sense. Worldwide, there are many examples of crystal-rich pumice - Toba, Fish Canyon Tuff, Bandelier Ignimbrites etc etc

Commented [JM26]: Your data set is incomplete so this statement is unwarranted. Also, you have not said whether crystallinity of pumiceous products have been corrected for vesicularity

Commented [JM27]: Text 605 - 612 should be omitted - (1) your data set is incomplete and (2) none of your samples have high (~50modal%) crystallinity

616 large volumes during Period II is similar to the description for the effusive volcanism of the Methana VF (Popa et al., 2020).
617 Popa et al. (2020) suggested that the critical factor controlling the effusive-explosive transitions of Methana is the crystallinity
618 of the erupted material based on their petrological data. The crystallinity has a higher influence on the bulk viscosity of magma
619 than the other factors (e.g. water content and composition; Popa et al., 2020). A higher crystallinity results in a slower ascent
620 velocity of magma and enhances the formation of permeable pathways in the conduit for the gas, which promotes the
621 outgassing of the magmas and leads to effusive behaviour. Lower crystallinity (<30 vol.%) of the magmas results in explosive
622 eruptions and has the opposite effect on outgassing, which causes high vesicularity of the eruption products.

623 Popa et al. (2020) showed that different magma plumbing systems are responsible for the explosive (crystal-poor) and effusive
624 (crystal-rich) eruptions of Methana (Popa et al., 2020, their Fig. 13). For the effusive lava domes of Period II, the composition
625 mainly ranges from basaltic-andesitic to dacitic, and the petrological observations of the dacite sample G15M0019 and 20 of
626 the Kantaro dome show the presence of olivine-clinopyroxene-orthopyroxene cumulates and amphibole-biotite reaction rims
627 (supplementary material I). The andesite of the Korakia dome (G15M0029) has a groundmass of acicular plagioclase and
628 plagioclase phenocrysts with sieve textures. These petrological observations suggest large-scale magma mixing between felsic
629 and more mafic magma, consistent with the hybridized magmas of the effusive events on Methana (e.g. Popa et al., 2020). The
630 pumiceous units of the explosive volcanoes on Milos during Period I and III could be caused by mafic magmas that intrude a
631 magma reservoir filled with felsic magma. This is consistent with the suggestion of Fytikas et al. (1986) that the main location
632 of feeding magma for the Milos VF is in the lower part of the crust from Pliocene to Pleistocene (\approx Period I).

633 It is noteworthy that the value of the Q_c ($0.2-4.7 \times 10^{-5} \text{ km}^3 \cdot \text{yr}^{-1}$) for the Milos VF is at least 2-3 orders lower than the average
634 for rhyolitic systems ($4.0 \times 10^{-3} \text{ km}^3 \cdot \text{yr}^{-1}$) and the mean for continental arcs ($\sim 70 \times 10^{-3} \text{ km}^3 \cdot \text{yr}^{-1}$) with a range of 8×10^{-6} –
635 $9 \times 10^{-2} \text{ km}^3 \cdot \text{yr}^{-1}$ (White et al., 2006). Milos overlaps with the lowest Q_c values of the study of White et al. (2006). For the
636 magma supply rate underneath the Milos VF, although no data are available for the ratio between intruded magma in the
637 crust below Milos and extruded volcanics (I:E). White et al. (2006) argued that a ratio of 5:1 (I:E) is probably a realistic
638 estimate for most volcanic centres and that this ratio can be higher in volcanic centres constructed on continental crust. This
639 would result in a magma supply rate from the mantle beneath the Milos VF could be estimated in the order of $0.1-3.3 \times 10^4$
640 $\text{km}^3 \cdot \text{yr}^{-1}$. Compared with other SAVA volcanic centres, Druitt et al. (2019) reported a long-term average magma supply rate
641 of approximately $1 \times 10^3 \text{ km}^3 \cdot \text{yr}^{-1}$ beneath the Kameni islands of Santorini, which is comparable to that of the Milos. Besides
642 the case of Santorini VF, no other information on the long-term average magma supply rate of other volcanic centres of the
643 SAVA is available to our knowledge.

644 Given that the island of Milos is approximately 15 km long (W-E), this results in a magma production rate over the last ~3.34
645 Ma of approximately $0.7-22 \text{ km}^3 \cdot \text{km}^{-1} \cdot \text{MyrMa}^{-1}$ can be estimated over the last ~3.34 Ma. Although this magma production
646 rate per km arc length is the onshore estimate for the Milos VF, it is still significantly lower than for oceanic arcs: $157-220$
647 $\text{km}^3 \cdot \text{MyrMa}^{-1} \cdot \text{km}^{-1}$ (Jicha and Jagoutz, 2015). For continental arcs the long-term magma production rate is more difficult to
648 establish because magmatism is cyclic, and short periods (5-20 Ma) of intense magmatism (“flare ups”) with 85
649 $\text{km}^3 \cdot \text{km}^{-1} \cdot \text{MyrMa}^{-1}$ are being alternated with periods of 25-50 Ma of low magma production rate of $20 \text{ km}^3 \cdot \text{km}^{-1}$
650 $\cdot \text{MyrMa}^{-1}$ (e.g. Jicha and Jagoutz, 2015). The periods of low magma production overlap with the magma production rates
651 beneath the Milos VF over the past ~3.34 Ma.

652 5 Conclusions

653 This study reports twenty-one new $^{40}\text{Ar}/^{39}\text{Ar}$ ages and major element data for 10 volcanic units of the Milos Volcanic Field.

654 In combination with previously published age data, geochemistry and facies analysis the following points can be made.

Commented [JM28]: this paper is not in reference list.

Commented [JM29]: correct only where crystallinity is very high - approaching 50 modal%

Commented [JM30]: 613-622 This text is not supported by data presented in this manuscript. Also, none of your samples have the high crystallinity (~50 modal%) claimed to be controlling eruption style. Also, you do not present any H₂O data so you cannot discount H₂O content as a primary control on eruption style.

Commented [JM31]: key data should be given in the data section, not in the supplement

Commented [JM32]: makes no sense

Commented [JM33]: this text is very hard to follow. I have tried to fix it up.

- 655 (1) The exact age of the start of volcanism in the Milos VF is still unclear due to the high degree of alteration of the oldest
656 deposits. The best estimate is based on our new $^{40}\text{Ar}/^{39}\text{Ar}$ ages, published K-Ar data and nannofossil biozones is
657 between 3.5 and 3.15 Ma.
- 658 (2) Based on the long-term volumetric volcanic output rate, the volcanic history of the Milos VF can be divided into two
659 slow growth periods, Period I (~3.3-2.1336 Ma) and III (1.48 Ma-present), and one relatively fast growth period,
660 Period II (2.1336-1.48 Ma).
- 661 ~~(3) Period I and III are dominated by low crystallinity, highly vesicular pumice deposits, whereas Period II is~~
662 ~~characterised by dominantly dome extrusions with low vesicular, high crystallinity products.~~
- 663 ~~(3) Large scale magma mixing between felsic and more mafic magma in the upper crust underneath Milos probably result~~
664 ~~in the high crystallinity of the effusively eruptive units of Period II. During Period I and III, the pumiceous units of~~
665 ~~the explosive volcanoes on Milos could be caused by mafic magma from deep that intrudes a magma reservoir filled~~
666 ~~with felsic magma. Period I and II are characterised by andesitic to rhyolitic lavas and pyroclastic units, whereas those~~
667 ~~of Period III are dominantly rhyolitic. The $\text{K}_2\text{O}/\text{SiO}_2$ ratio is constant over the 3.3 Ma history of the Milos VF. The~~
668 ~~evolution of the Milos VF volcanic rocks changed over time in composition from basaltic-andesite-rhyolite volcanism~~
669 ~~to mainly rhyolite.~~
- 670 (4) The ~~long-term~~long-term volumetric volcanic output rate of Milos is $0.2\text{-}4.7 \times 10^{-5} \text{ km}^3 \cdot \text{yr}^{-1}$, ~~2-3~~two-three orders of
671 magnitude lower than the average for rhyolitic systems and continental arcs.

672

673 Acknowledgement

674 We would like to thank Roel van Elsas with the assistance of rock crushing and mineral separation. Kiki Dings helped with
675 the XRF bead preparation and measurements. Lara Borst and Onno Postma assisted with the $^{40}\text{Ar}/^{39}\text{Ar}$ dating. We acknowledge
676 the Greek Institute of Geology and Mineral Exploration (IGME) for permission to conduct fieldwork on Milos. Xiaolong Zhou
677 would like to acknowledge a grant no. 201506400055 from the China Scholarship Council (CSC). The $^{40}\text{Ar}/^{39}\text{Ar}$ facility of the
678 VU is covered by NWO grant 834.09.004. This research benefitted from funding from the European Research Council under
679 the European Union's Seventh Framework Programme (FP7/2007-2013)/ERC grant agreement n° 319209. A previous version
680 of this manuscript greatly benefitted from a very detailed and constructive review by Dr. J. McPhie. A second review by Dr J.
681 McPhie, Dr. J-F. Wotzlaw and Dr. Peter Abbott helped to clarify the interpretation of the geochronology of Milos. We thank
682 Drs. J. Nadden, J. Miles and S Tapster for pointing out mistakes in our figures.

683
684

685 **References**

- 686 Alfieris, D., Voudouris, P. and Spry, P. G.: Shallow submarine epithermal Pb-Zn-Cu-Au-Ag-Te mineralization on western
687 Milos Island, Aegean Volcanic Arc, Greece: Mineralogical, geological and geochemical constraints, *Ore Geol. Rev.*, 53,
688 159–180, doi:10.1016/j.oregeorev.2013.01.007, 2013.
- 689 Angelier, J., Cantagrel, J.-M. and Vilminot, J.-C.: Neotectonique cassante et volcanisme plio-quadernaire dans l'arc egeen
690 interne; l'île de Milos (Grece), *Bull. la Société Géologique Fr.*, 7(1), 119–124, 1977.
- 691 Arias, A., Oddone, M., Bigazzi, G., Di Muro, A., Principe, C. and Norelli, P.: New data for the characterization of Milos
692 obsidians, *J. Radioanal. Nucl. Chem.*, 268(2), 371–386, doi:10.1007/s10967-006-0183-9, 2006.
- 693 Berger, G. W. and York, D.: Geothermometry from $^{40}\text{Ar}/^{39}\text{Ar}$ dating experiments, *Geochim. Cosmochim. Acta*, 45(6), 795–
694 811, doi:10.1016/0016-7037(81)90109-5, 1981.
- 695 Bigazzi, G. and Radi, G.: Datazione con le tracce di fissione per l'identificazione della provenienza dei manufatti di
696 ossidiana, *Riv. di Sci. Preist.*, 36/1–2, 223–250, 1981.
- 697 Calvo, J. P., Triantaphyllou, M. V., Regueiro, M. and Stamatakis, M. G.: Alternating diatomaceous and volcanoclastic
698 deposits in Milos Island, Greece. A contribution to the upper Pliocene-lower Pleistocene stratigraphy of the Aegean Sea,
699 *Palaeogeogr. Palaeoclimatol. Palaeoecol.*, 321–322, 24–40, doi:10.1016/j.palaeo.2012.01.013, 2012.
- 700 Campos Venuti, M. and Rossi, P. L.: Depositional facies in the Fyriplaka rhyolitic tuff ring, Milos Island (Cyclades, Greece),
701 *Acta Vulcanol.*, 8, 173–192, 1996.
- 702 Cassata, W. S. and Renne, P. R.: Systematic variations of argon diffusion in feldspars and implications for
703 thermochronometry, *Geochim. Cosmochim. Acta*, 112, 251–287, doi:10.1016/j.gca.2013.02.030, 2013.
- 704 Cole, P. D., Calder, E. S., Sparks, R. S. J., Clarke, A. B., Druitt, T. H., Young, S. R., Herd, R. A., Harford, C. L. and Norton,
705 G. E.: Deposits from dome-collapse and fountain-collapse pyroclastic flows at Soufrière Hills Volcano, Montserrat, *Geol.*
706 *Soc. London, Mem.*, 21(1), 231–262, 2002.
- 707 Crossweller, H. S., Arora, B., Brown, S. K., Cottrell, E., Deligne, N. I., Guerrero, N. O., Hobbs, L., Kiyosugi, K., Loughlin,
708 S. C. and Lowndes, J.: Global database on large magnitude explosive volcanic eruptions (LaMEVE), *J. Appl. Volcanol.*,
709 1(1), 4, 2012.
- 710 Druitt, T. H., Edwards, L., Mellors, R. M., Pyle, D. M., Sparks, R. S. J., Lanphere, M., Davies, M. and Barreiro, B.:
711 Santorini Volcano, *Geol. Soc. Mem.*, 19 [online] Available from: <http://pubs.er.usgs.gov/publication/70094778>, 1999.
- 712 Druitt, T. H., Pyle, D. M. and Mather, T. A.: Santorini Volcano and its Plumbing System, *Elements*, 15(3), 177–184,
713 doi:10.2138/gselements.15.3.177, 2019.
- 714 Duermeijer, C. E., Nyst, M., Meijer, P. T., Langereis, C. G. and Spakman, W.: Neogene evolution of the Aegean arc:
715 Paleomagnetic and geodetic evidence for a rapid and young rotation phase, *Earth Planet. Sci. Lett.*, 176(3–4), 509–525,
716 doi:10.1016/S0012-821X(00)00023-6, 2000.
- 717 Ferrara, G., Fytikas, M., Giuliani, O. and Marinelli, G.: Age of the formation of the Aegean active volcanic arc, *Thera*
718 *Aegean world II*, 2, 37–41, 1980.
- 719 Flowers, R. M., Bowring, S. A., Tulloch, A. J. and Klepeis, K. A.: Tempo of burial and exhumation within the deep roots of
720 a magmatic arc, Fiordland, New Zealand, *Geology*, 33(1), 17–20, doi:10.1130/G21010.1, 2005.
- 721 Francalanci, L. and Zellmer, G. F.: Magma Genesis at the South Aegean Volcanic Arc, *Elements*, 15(3), 165–170,
722 doi:10.2138/gselements.15.3.165, 2019.
- 723 Francalanci, L., Vougioukalakis, G. E., Fytikas, M., Beccaluva, L., Bianchini, G. and Wilson, M.: Petrology and
724 volcanology of Kimolos and Polyegos volcanoes within the context of the South Aegean arc, Greece, *Spec. Pap. Soc. Am.*,
725 418, 33, 2007.
- 726 Frey, H. M., Lange, R. A., Hall, C. M. and Delgado-Granados, H.: Magma eruption rates constrained by $^{40}\text{Ar}/^{39}\text{Ar}$
727 chronology and GIS for the Ceboruco-San Pedro volcanic field, western Mexico, *Bull. Geol. Soc. Am.*, 116(3–4), 259–276,

728 doi:10.1130/B25321.1, 2004.

729 Fytikas, M., Giuliani, O., Innocenti, F., Marinelli, G. and Mazzuoli, R.: Geochronological data on recent magmatism of the
730 Aegean Sea, *Tectonophysics*, 31(1–2), T29–T34, doi:10.1016/0040-1951(76)90161-X, 1976.

731 Fytikas, M., 1977. *Geology and Geothermics of Milos Island*. Thesis, Thessaloniki University, 228 pp. (in Greek with
732 English summary).

733 Fytikas, M., Innocenti, F., Kolios, N., Manetti, P., Mazzuoli, R., Poli, G., Rita, F. and Villari, L.: Volcanology and petrology
734 of volcanic products from the island of Milos and neighbouring islets, *J. Volcanol. Geotherm. Res.*, 28(3–4), 297–317,
735 doi:10.1016/0377-0273(86)90028-4, 1986.

736 Fytikas, M.: Updating of the geological and geothermal research on Milos island, *Geothermics*, 18(4), 485–496,
737 doi:10.1016/0375-6505(89)90051-5, 1989.

738 Grasemann, B., Huet, B., Schneider, D. A., Rice, A. H. N., Lemonnier, N. and Tschegg, C.: Miocene postorogenic extension
739 of the Eocene synorogenic imbricated Hellenic subduction channel: New constraints from Milos (Cyclades, Greece), *Bull.*
740 *Geol. Soc. Am.*, 130(1–2), 238–262, doi:10.1130/B31731.1, 2018.

741 Grove, M. and Harrison, T. M.: $^{40}\text{Ar}^*$ diffusion in Fe-rich biotite, *Am. Mineral.*, 81(7–8), 940–951, 1996.

742 Hayes, G. P., Moore, G. L., Portner, D. E., Hearne, M., Flamme, H., Furtney, M. and Smoczyk, G. M.: Slab2, a
743 comprehensive subduction zone geometry model, *Science* (80-.), 362(6410), 58–61, doi:10.1126/science.aat4723, 2018.

744 Hildreth, W. and Lanphere, M. A.: Potassium-argon geochronology of a basalt-andesite-dacite arc system: The Mount
745 Adams volcanic field, Cascade Range of southern Washington, *Geol. Soc. Am. Bull.*, 106(11), 1413–1429, 1994.

746 Hildreth, W., Fierstein, J. and Lanphere, M.: Eruptive history and geochronology of the Mount Baker volcanic field,
747 Washington, *Geol. Soc. Am. Bull.*, 115(6), 729–764, 2003a.

748 Hildreth, W., Lanphere, M. A. and Fierstein, J.: Geochronology and eruptive history of the Katmai volcanic cluster, Alaska
749 Peninsula, *Earth Planet. Sci. Lett.*, 214(1–2), 93–114, doi:10.1016/S0012-821X(03)00321-2, 2003b.

750 Van Hinsbergen, D. J. J., Snel, E., Garstman, S. A., Marunțeanu, M., Langereis, C. G., Wortel, M. J. R. and Meulenkaamp, J.
751 E.: Vertical motions in the Aegean volcanic arc: Evidence for rapid subsidence preceding volcanic activity on Milos and
752 Aegina, *Mar. Geol.*, 209(1–4), 329–345, doi:10.1016/j.margeo.2004.06.006, 2004.

753 Hora, J. M., Singer, B. S., Jicha, B. R., Beard, B. L., Johnson, C. M., de Silva, S. and Salisbury, M.: Volcanic biotite-
754 sanidine $^{40}\text{Ar}/^{39}\text{Ar}$ age discordances reflect Ar partitioning and pre-eruption closure in biotite, *Geology*, 38(10), 923–926,
755 doi:10.1130/G31064.1, 2010.

756 Ilst, L.: A laboratory overflow-centrifuge for heavy liquid mineral separation, *Am. Mineral.*, 58, 1088–1093, 1973.

757 Jicha, B. R. and Jagoutz, O.: Magma production rates for intraoceanic arcs, *Elements*, 11(2), 105–112,
758 doi:10.2113/gselements.11.2.105, 2015.

759 Kiliass, S. P., Naden, J., Cheliotis, I., Shepherd, T. J., Constandinidou, H., Crossing, J. and Simos, I.: Epithermal gold
760 mineralisation in the active Aegian volcanic arc: The Profitis Ilias deposits, Milos Island, Greece, *Miner. Depos.*, 36(1), 32–
761 44, doi:10.1007/s001260050284, 2001.

762 Koppers, A. A. P.: ArArCALC-software for $^{40}\text{Ar}/^{39}\text{Ar}$ age calculations, *Comput. Geosci.*, 28(5), 605–619,
763 doi:10.1016/S0098-3004(01)00095-4, 2002.

764 Kornprobst, J., Kienast, J.-R. and Vilminot, J.-C.: The high-pressure assemblages at Milos, Greece, *Contrib. to Mineral.*
765 *Petrol.*, 69(1), 49–63, doi:10.1007/bf00375193, 1979.

766 Kuiper, K. F., Deino, A., Hilgen, F. J., Krijgsman, W., Renne, P. R. and Wijbrans, J. R.: Synchronizing Rock Clocks of
767 Earth History, *Science* (80-.), 320(5875), 500–504, doi:10.1126/science.1154339, 2008.

768 Lee, J. K. W.: Ar–Ar and K–Ar Dating BT - *Encyclopedia of Scientific Dating Methods*, edited by W. Jack Rink and J. W.
769 Thompson, pp. 58–73, Springer Netherlands, Dordrecht., 2015.

770 Lee, J. Y., Marti, K., Severinghaus, J. P., Kawamura, K., Yoo, H. S., Lee, J. B. and Kim, J. S.: A redetermination of the

771 isotopic abundances of atmospheric Ar, *Geochim. Cosmochim. Acta*, 70(17), 4507–4512, doi:10.1016/j.gca.2006.06.1563,
772 2006.

773 Mark, D. F., Barfod, D., Stuart, F. M. and Imlach, J.: The ARGUS multicollector noble gas mass spectrometer: Performance
774 for 40Ar/39Ar geochronology, *Geochemistry, Geophys. Geosystems*, 10(10), 1–9, doi:10.1029/2009GC002643, 2009.

775 Matsuda, J., Senoh, K., Maruoka, T., Sato, H. and Mitropoulos, P.: K-Ar ages of the Aegean the volcanic rocks and arc-
776 trench system their implication for the arc-trench system, *Geochem. J.*, 33, 369–377, 1999.

777 McKenzie, D.: Active tectonics of the Alpine—Himalayan belt: the Aegean Sea and surrounding regions, *Geophys. J. Int.*,
778 55(1), 217–254, 1978.

779 Meulenkaamp, J. E., Wortel, M. J. R., van Wamel, W. A., Spakman, W. and Hoogerduyn Strating, E.: On the Hellenic
780 subduction zone and the geodynamic evolution of Crete since the late Middle Miocene, *Tectonophysics*, 146(1–4), 203–215,
781 doi:10.1016/0040-1951(88)90091-1, 1988.

782 Min, K., Mundil, R., Renne, P. R. and Ludwig, K. R.: A test for systematic errors in 40Ar/39Ar geochronology, *Geochim.*
783 *Cosmochim. Acta*, 64(1), 73–98, 2000.

784 Nicholls, I. A.: Santorini volcano, greece - tectonic and petrochemical relationships with volcanics of the Aegean region,
785 *Tectonophysics*, 11(5), 377–385, doi:10.1016/0040-1951(71)90026-6, 1971.

786 Pe-Piper, G. and Piper, D. J. W.: The South Aegean active volcanic arc: relationships between magmatism and tectonics,
787 *Dev. Volcanol.*, 7(C), 113–133, doi:10.1016/S1871-644X(05)80034-8, 2005.

788 Pe-Piper, G. and Piper, D. J. W.: Neogene backarc volcanism of the Aegean: New insights into the relationship between
789 magmatism and tectonics, *Geol. Soc. Am. Spec. Pap.*, 418(02), 17–31, doi:10.1130/2007.2418(02), 2007.

790 Pe-Piper, G. and Piper, D. J. W.: The effect of changing regional tectonics on an arc volcano: Methana, Greece, *J. Volcanol.*
791 *Geotherm. Res.*, 260, 146–163, doi:10.1016/j.jvolgeoes.2013.05.011, 2013.

792 [Principe C. Arias A. Zoppi U.: Origin, transport and deposition of a debris avalanche de- posit of phreatic origin on Milos](#)
793 [Island \(Greece\). Montagne Pelee 1902-2002, Explosive Vol- canism in Subduction Zones, Martinique 12-16 May,](#)
794 [2002. Abstracts p. 71, 2002.](#)

795 Raffi, I., Wade, B. S., Pálike, H., Beu, A. G., Cooper, R., Crundwell, M. P., Krijgsman, W., Moore, T., Raine, I. and
796 Sardella, R.: The Neogene Period, in *Geologic Time Scale 2020*, pp. 1141–1215, Elsevier., 2020.

797 Rinaldi, M. and Venuti, M. C.: The submarine eruption of the Bombarda volcano, Milos Island, Cyclades, Greece, *Bull.*
798 *Volcanol.*, 65(4), 282–293, doi:10.1007/s00445-002-0260-z, 2003.

799 Rivera, T. A., Storey, M., Zeeden, C., Hilgen, F. J. and Kuiper, K.: A refined astronomically calibrated 40Ar/39Ar age for
800 Fish Canyon sanidine, *Earth Planet. Sci. Lett.*, 311(3–4), 420–426, doi:10.1016/j.epsl.2011.09.017, 2011.

801 Rontogianni, S., Konstantinou, N. S., Melis, C. P. and Evangelidis: Slab stress field in the Hellenic subduction zone as
802 inferred from intermediate-depth earthquakes, *Earth, Planets Sp.*, 63(2), 139–144, doi:10.5047/eps.2010.11.011, 2011.

803 Schaen, A., Jicha, B., Hodges, K., Vermeesch, P., Stelten, M., Mercer, C., Phillips, D., Rivera, T., Jourdan, F., Matchan, E.,
804 Hemming, S., Morgan, L., Kelley, S., Cassata, W., Heizler, M., Vasconcelos, P., Benowitz, J., Koppers, A., Mark, D.,
805 Niespolo, E., Sprain, C., Hames, W., Kuiper, K., Turrin, B., Renne, P., Ross, J., Nomade, S., Guillou, H., Webb, L., Cohen,
806 B., Calvert, A., Joyce, N., Ganerød, M., Wijbrans, J., Ishizuka, O., He, H., Ramirez, A., Pfänder, J., Lopez-Martínez, M.,
807 Qiu, H. and Singer, B.: Interpreting and reporting 40Ar/39Ar geochronologic data, *GSA Bull.*, doi:10.1130/B35560.1, 2020.

808 Singer, B. S., Thompson, R. A., Dungan, M. A., Feeley, T. C., Nelson, S. T., Pickens, J. C., Brown, L. L., Wulff, A. W.,
809 Davidson, J. P. and Metzger, J.: Volcanism and erosion during the past 930 k.y. at the Tatará–San Pedro complex, Chilean
810 Andes, *Geol. Soc. Am. Bull.*, 109(2), 127–142, doi:10.1130/0016-7606(1997)109<0127:VAEDTP>2.3.CO;2, 1997.

811 Sonder, R. A.: Zur Geologie and Petrographie der Inselgruppe von Milos, *Zeitschr. Volc.*, 8, 11–231, 1924.

812 Spakman, W., Wortel, M. J. R. and Vlaar, N. J.: The Hellenic Subduction Zone: A tomographic image and its geodynamic
813 implications, *Geophys. Res. Lett.*, 15(1), 60–63, doi:10.1029/GL015i001p00060, 1988.

814 Stewart, A. L.: Volcanic Facies Architecture and Evolution of Milos, Greece, University of Tasmania., 2003.
815 Stewart, A. L. and McPhie, J.: Internal structure and emplacement of an Upper Pliocene dacite cryptodome, Milos Island,
816 Greece, *J. Volcanol. Geotherm. Res.*, 124(1–2), 129–148, doi:10.1016/S0377-0273(03)00074-X, 2003.
817 Stewart, A. L. and McPhie, J.: An Upper Pliocene coarse pumice breccia generated by a shallow submarine explosive
818 eruption, Milos, Greece, *Bull. Volcanol.*, 66(1), 15–28, doi:10.1007/s00445-003-0292-z, 2004.
819 Stewart, A. L. and McPhie, J.: Facies architecture and Late Pliocene – Pleistocene evolution of a felsic volcanic island,
820 Milos, Greece, *Bull. Volcanol.*, 68(7–8), 703–726, doi:10.1007/s00445-005-0045-2, 2006.
821 Traineau, H. and Dalabakis, P.: Mise en evidence d’une eruption phreatique historique sur l’île de Milos (Grece), *CR Acad*
822 *Sci Paris*, 1–38, 1989.
823 Vougioukalakis, G. E., Satow, C. G. and Druitt, T. H.: Volcanism of the South Aegean volcanic arc, *Elements*, 15(3), 159–
824 164, 2019.
825 Wendt, I. and Carl, C.: The statistical distribution of the mean squared weighted deviation, *Chem. Geol. Isot. Geosci. Sect.*,
826 86(4), 275–285, doi:10.1016/0168-9622(91)90010-T, 1991.
827 White, S. M., Crisp, J. A. and Spera, F. J.: Long-term volumetric eruption rates and magma budgets, *Geochemistry,*
828 *Geophys. Geosystems*, 7(3), 262–266, doi:10.1029/2005GC001002, 2006.
829 York, D.: Least squares fitting of a straight line with correlated errors, *Earth Planet. Sci. Lett.*, 5(C), 320–324,
830 doi:10.1016/s0012-821x(68)80059-7, 1968.
831

Table 1. Published eruption ages of stratigraphic units of the island of Milos

Stratigraphy	Sample	Mineral	Location	Petrology	K ₂ O (wt.%)	Age (Ma)	±1σ
Unit IV	⁴⁰ Angelier_1	Unknown	Fyriplaka	Rhyolite	-	-	-
Unit III	⁴⁰ Angelier_2	Unknown	Halepa	Rhyolite	2.44	0.95	0.06
Unit II	⁴⁰ Angelier_3	Unknown	Triades	Dacite	1.47	1.71	0.08
	⁴⁰ Angelier_4	Unknown	Kleftico	Andesite	1.77	2.33	0.09
	⁴⁰ Angelier_5	Unknown	Kleftico	Andesite	1.45	2.50	0.09
Unit I	⁴⁰ Angelier_6	Unknown	Adamas	Rhyolite	2.90	2.15	0.08
	⁴⁰ Angelier_7	Unknown	Dhemeneghaki	Rhyolite	2.75	1.84	0.08
Phreatic activity	⁶ Gif-7358&7359	Carbonized wood	Agia-Kiriaki	Lahar deposits	-	200 BC-200 AD	
CFT	²³⁸ M196	Unknown	Fyriplaka	Rhyolite	2.9	0.09	0.02
	²³⁸ M194	Unknown	Fyriplaka	Rhyolite	2.85	0.14	0.03
	²³⁸ M168	Unknown	Trachilas	Rhyolite	3.91	0.37	0.09
	²³⁸ M-48	Biotite	NW of Filiplaka	Rhyolite	6.41	0.48	0.05
PSLD	²³⁸ M1-1	Lava	Plakes	Dacite	2.07	0.80	0.10
	²³⁸ M-OB1	Groundmass	N of Dhemenegaki	Obsidian	2.53	0.88	0.18
	²³⁸ M27	Unknown	Plakes	Dacite	1.87	0.97	0.06
	²³⁸ M1-4	Lava	Plakes	Dacite	2.32	1.20	0.10
	⁴⁰ MIL130	Zircon	Triades	Dacite	-	1.44	0.08
	²³⁸ M-OB2	Groundmass	Bombarda	Obsidian	2.73	1.47	0.05
	⁶ Fission track1	Groundmass	Adamas	Obsidian	-	1.54	0.18
	⁶ Fission track2	Groundmass	Bombarda	Obsidian	-	1.57	0.15
	²³⁸ Fission track3	Groundmass	Bombarda-Adamas	Obsidian	-	1.57	0.12
	²³⁸ M103	Unknown	near Pollonia	Andesite	1.87	1.59	0.25
	²³⁸ Fission track3	Groundmass	Dhemeneghaki	Obsidian	-	1.60	0.06
CDLF	²³⁸ M146	Unknown	1km NW of Adamas	Rhyolite	3.09	1.71	0.05
	²³⁸ M110	Unknown	Sarakimiko	Dacite	2.57	1.85	0.10
	²³⁸ M1	Unknown	Aghios, near Triades	Rhyolite	3.32	2.04	0.09
	²³⁸ M66	Unknown	~1 km NW of Adamas	Dacite	2.61	2.03	0.06
	⁴⁰ MIL243	Zircon	Triades	Dacite	-	2.18	0.09
	²³⁸ M156	Unknown	Angathia, near Triades	Dacite	2.84	2.38	0.10
BPS	⁴⁰ MIL265	Zircon	Filakopi	Rhyolite	-	2.66	0.07
	⁴⁰ MIL343	Zircon	Kalogeros-cryptodome	Dacite	-	2.70	0.04
	²³⁸ M164	Unknown	Kleftico	Rhyolite	2.84	3.08	0.08
	²³⁸ M163	Unknown	Kleftico	Andesite	1.18	3.50	0.14

Commented [PA34]: Instead of using the referring to the original references here using the superscripts, please add them in a separate column

Table 1. Published eruption ages of stratigraphic units of the island of Milos

Stratigraphy	Sample	Mineral	Location	Petrology	K ₂ O (wt.%)	Age (Ma)	±1σ	Reference
Unit IV	Angelier_1	Unknown	Fyriplaka	Rhyolite	=	=	=	
Unit III	Angelier_2	Unknown	Halepa	Rhyolite	2.44	0.95	0.06	
Unit II	Angelier_3	Unknown	Triades	Dacite	1.47	1.71	0.08	Angelier et al. (1977)
	Angelier_4	Unknown	Kleftico	Andesite	1.77	2.33	0.09	
	Angelier_5	Unknown	Kleftico	Andesite	1.45	2.50	0.09	
Unit I	Angelier_6	Unknown	Adamas	Rhyolite	2.90	2.15	0.08	Trainau and Dalabakis (1989)
	Angelier_7	Unknown	Dhemeneghaki	Rhyolite	2.75	1.84	0.08	
Phreatic activity	Gif-7358&7359	Carbonized wood	Agia Kiriaki	Lahar deposits	=	200 BC-200 AD		
CFT	M196	Unknown	Fyriplaka	Rhyolite	2.9	0.09	0.02	Fytikas et al. (1976, 1986)
	M194	Unknown	Fyriplaka	Rhyolite	2.85	0.14	0.03	
	M168	Unknown	Trachilas	Rhyolite	3.91	0.37	0.09	
	M-48	Biotite	NW of Filiplaka	Rhyolite	6.41	0.48	0.05	
PSLD	M-OB1	Groundmass	N of Dhemenegaki	Obsidian	2.53	0.88	0.18	
	M27	Unknown	Plakes	Dacite	1.87	0.97	0.06	

	<u>M-OB2</u>	<u>Groundmass</u>	<u>Bombarda</u>	<u>Obsidian</u>	<u>2.73</u>	<u>1.47</u>	<u>0.05</u>	
	<u>M103</u>	<u>Unknown</u>	<u>near Pollonia</u>	<u>Andesite</u>	<u>1.87</u>	<u>1.59</u>	<u>0.25</u>	<u>Fytikas et al. (1976, 1986)</u>
	<u>M146</u>	<u>Unknown</u>	<u>1km NW of Adamas</u>	<u>Rhyolite</u>	<u>3.09</u>	<u>1.71</u>	<u>0.05</u>	
	<u>M110</u>	<u>Unknown</u>	<u>Sarakiniko</u>	<u>Dacite</u>	<u>2.57</u>	<u>1.85</u>	<u>0.10</u>	
	<u>MI-1</u>	<u>Lava</u>	<u>Plakes</u>	<u>Dacite</u>	<u>2.07</u>	<u>0.80</u>	<u>0.10</u>	<u>Matsuda et al. (1999)</u>
	<u>MI-4</u>	<u>Lava</u>	<u>Plakes</u>	<u>Dacite</u>	<u>2.32</u>	<u>1.20</u>	<u>0.10</u>	
	<u>MIL130</u>	<u>Zircon</u>	<u>Triades</u>	<u>Dacite</u>	<u>-</u>	<u>1.44</u>	<u>0.08</u>	<u>Stewart and McPhie (2006)</u>
	<u>Fission track1</u>	<u>Groundmass</u>	<u>Adamas</u>	<u>Obsidian</u>	<u>-</u>	<u>1.54</u>	<u>0.18</u>	<u>Bigazzi and Radi (1981)</u>
	<u>Fission track2</u>	<u>Groundmass</u>	<u>Bombarda</u>	<u>Obsidian</u>	<u>-</u>	<u>1.57</u>	<u>0.15</u>	
	<u>Fission track3</u>	<u>Groundmass</u>	<u>Bombarda-Adamas</u>	<u>Obsidian</u>	<u>-</u>	<u>1.57</u>	<u>0.12</u>	<u>Arias et al. (2006)</u>
	<u>Fission track3</u>	<u>Groundmass</u>	<u>Dhemeneghaki</u>	<u>Obsidian</u>	<u>-</u>	<u>1.60</u>	<u>0.06</u>	
	<u>M1</u>	<u>Unknown</u>	<u>Aghios, near Triades</u>	<u>Rhyolite</u>	<u>3.32</u>	<u>2.04</u>	<u>0.09</u>	<u>Fytikas et al. (1976, 1986)</u>
	<u>M66</u>	<u>Unknown</u>	<u>~1 km NW of Adamas</u>	<u>Dacite</u>	<u>2.61</u>	<u>2.03</u>	<u>0.06</u>	
<u>CDLF</u>	<u>M156</u>	<u>Unknown</u>	<u>Angathia, near Triades</u>	<u>Dacite</u>	<u>2.84</u>	<u>2.38</u>	<u>0.10</u>	
	<u>MIL243</u>	<u>Zircon</u>	<u>Triades</u>	<u>Dacite</u>	<u>-</u>	<u>2.18</u>	<u>0.09</u>	<u>Stewart and McPhie (2006)</u>
	<u>MIL365</u>	<u>Zircon</u>	<u>Filakopi</u>	<u>Rhyolite</u>	<u>-</u>	<u>2.66</u>	<u>0.07</u>	<u>Stewart and McPhie (2006)</u>
<u>BPS</u>	<u>MIL343</u>	<u>Zircon</u>	<u>Kalogeros cryptodome</u>	<u>Dacite</u>	<u>-</u>	<u>2.70</u>	<u>0.04</u>	
	<u>M164</u>	<u>Unknown</u>	<u>Kleftico</u>	<u>Rhyolite</u>	<u>2.84</u>	<u>3.08</u>	<u>0.08</u>	<u>Fytikas et al. (1976, 1986)</u>
	<u>M163</u>	<u>Unknown</u>	<u>Kleftico</u>	<u>Andesite</u>	<u>1.18</u>	<u>3.50</u>	<u>0.14</u>	

Published ages from 1=Angelier et al. (1977), 2=Fytikas et al. (1976, 1986), 3=Matsuda et al. (1999), 4=Stewart and McPhie (2006), 5=Trainau and Dalabakis (1989), 6=Bigazzi and Radi (1981), Arias et al. (2006). Angelier et al. (1977) do not provide sample names, only numbers for the sample locations. Here the location is given after "Angelier_" (Angelier et al. 1977, their Fig. 3). Abbreviations: BPS=Basal pyroclastic series; CDLF=Complex of domes and lava flows; PS LD=Pyroclastic series and lava domes; CTF=Complexes of Trachilas and Fyriplaka. See more details in Fig. 4.

Table 2. Incremental heating $^{40}\text{Ar}/^{39}\text{Ar}$ results of the Milos volcanic field.

Volcanic Unit	Sample -ID	Irr-ID	Latitude	Age $\pm 1\sigma$ (Ma)	MS WD	$^{39}\text{Ar}_{\text{K}}$ (%)	n/ntotal	$^{40}\text{Ar}^*$ (%)	K/Ca $\pm 1\sigma$	Inverse isochron age (Ma)	$^{40}\text{Ar}/^{36}\text{Ar} \pm 1\sigma$	MS WD
Fyriplaka Complex	G15M0 008 ^b	VU110-Z22a	36.6729 N 24.4670 E	0.05 \pm 0.01	0.04	16.24	3/15	1.20	60.9 \pm 10.6	0.05 \pm 0.10	298.08 \pm 8.77	0.08
		VU110-Z22b		0.062 \pm 0.003	0.91	71.81	8/11	2.69	57.3 \pm 8.4	0.06 \pm 0.02	299.39 \pm 3.66	1.09
		Combined (Z22)		0.061 \pm 0.004	0.82	41.37	11/26	2.29	58.0 \pm 6.3	0.07 \pm 0.01	296.78 \pm 1.78	0.83
	G15M0 012 ^b	VU110-Z24a	36.6795 N 24.4828 E	0.05 \pm 0.01	3.09	38.89	3/11	2.89	40.0 \pm 6.0	0.14 \pm 0.03	285.98 \pm 4.76	0.07
		VU110-Z24b		0.09 \pm 0.02	8.16	48.04	4/11	4.59	30.1 \pm 7.1	0.09 \pm 0.05	297.46 \pm 10.29	12.78
		Combined (Z24)		0.07 \pm 0.01	7.44	43.53	7/22	3.86	32.3 \pm 5.0	0.09 \pm 0.03	295.67 \pm 7.39	9.02
	G15M0 009 ^b	VU110-Z23a	36.6716 N 24.4891 E	0.11 \pm 0.02	1.37	18.33	4/12	1.65	45.4 \pm 7.3	0.76 \pm 0.30	268.52 \pm 17.08	0.90
		VU110-Z23b		0.11 \pm 0.03	6.77	41.05	4/11	3.13	19.4 \pm 3.7	0.29 \pm 0.14	285.17 \pm 15.80	8.09
		Combined (Z23)		0.11 \pm 0.02	3.50	29.50	8/21	2.39	19.7 \pm 2.6	0.15 \pm 0.05	295.78 \pm 4.34	4.04
Trachilas Complex	G15M0 007 ^b	VU110-Z12a	36.7671 N 24.4124 E	0.30 \pm 0.01	4.61	56.50	8/16	14.51	38.3 \pm 2.4	0.28 \pm 0.05	301.42 \pm 9.01	5.47
		VU110-Z12b		0.317 \pm 0.004	1.29	74.05	4/11	18.30	32.0 \pm 2.5	0.31 \pm 0.03	299.52 \pm 6.40	2.04
		Combined (Z12)		0.31 \pm 0.01	5.57	65.27	12/27	15.77	33.1 \pm 1.6	0.34 \pm 0.03	293.05 \pm 5.50	5.84
Kontaro dome	G15M0 020 ^c	VU108-Z5a_5		1.52 \pm 0.01	1.06	61.82	8/12	18.30	1.51 \pm 0.05	1.49 \pm 0.02	300.03 \pm 0.86	0.95
		VU108-Z5b_1	36.7234 N 24.3952 E	1.56 \pm 0.01	1.94	41.54	3/10	47.94	1.73 \pm 0.06	1.58 \pm 0.02	294.97 \pm 3.74	2.17
		VU108-Z5b_2		1.52 \pm 0.01	1.73	62.45	5/10	22.95	1.56 \pm 0.08	1.53 \pm 0.02	298.12 \pm 0.89	2.34
		Combined (Z5)		1.54 \pm 0.01	3.06	57.32	16/32	25.31	1.58 \pm 0.04	1.55 \pm 0.01	297.41 \pm 0.57	2.82
	G15M0 019 ^c	VU108-Z6a_4		1.62 \pm 0.01	3.80	89.75	9/11	34.28	0.91 \pm 0.05	1.62 \pm 0.02	297.66 \pm 1.36	4.40
		VU108-Z6a_5	36.7211 N 24.3950 E	1.55 \pm 0.01	4.50	95.41	10/12	35.26	0.88 \pm 0.06	1.55 \pm 0.01	298.73 \pm 1.29	5.40
		VU108-Z6b_1		1.56 \pm 0.01	4.05	56.64	4/10	53.19	1.02 \pm 0.01	1.48 \pm 0.02	315.46 \pm 5.20	0.44
Combined (Z6)		1.55 \pm 0.01	5	80.97	27/45	38.78	0.93 \pm 0.04	1.53 \pm 0.02	300.60 \pm 2.27	34.25		
Dheme-neghaki volcano	G15M0 032B ^d	VU108-Z18	36.7084 N 24.5324 E	1.825 \pm 0.002	0.91	98.64	12/13	93.86	1.83 \pm 0.04	1.825 \pm 0.003	301.52 \pm 3.34	0.93
Triades lava dome	G15M0 021 ^b	VU110-Z4_2		1.97 \pm 0.01	1.66	63.83	4/12	54.72	107.55 \pm 20.64	1.97 \pm 0.03	299.16 \pm 5.36	2.56
		VU110-Z4_2b	36.7402 N 24.3397 E	2.01 \pm 0.01	6.76	75.39	6/16	57.84	54.43 \pm 8.29	2.04 \pm 0.05	293.08 \pm 10.44	8.15
		Combined (Z4)		1.99 \pm 0.01	9.08	69.12	10/28	56.59	73.52 \pm 6.46	2.00 \pm 0.04	295.64 \pm 7.89	10.30
Adamas lava dome	G15M0 004 ^a	VU108-Z10_1		2.99 \pm 0.11	1.00	87.31	4/12	16.36	0.030 \pm 0.002	7.89 \pm 2.46	202.39 \pm 48.47	0.01
		VU108-Z10_2	36.7282 N 24.4315 E	2.86 \pm 0.09	1.50	86.18	7/11	17.58	0.029 \pm 0.002	0.70 \pm 0.29	348.91 \pm 27.33	1.00
		Combined (Z10)		2.90 \pm 0.07	1.31	86.74	11/23	17.13	0.029 \pm 0.001	1.95 \pm 0.45	319.51 \pm 14.70	1.17
The dyke of Mavro Vouni lava dome	G15M0 016 ^c	VU108-Z8a		2.71 \pm 0.02	2.31	79.64	8/12	16.57	0.24 \pm 0.05	2.65 \pm 0.10	299.84 \pm 2.32	2.92
		VU108-Z8a_4	36.6668 N 24.3398 E	2.61 \pm 0.03	0.93	57.41	7/12	16.86	0.12 \pm 0.07	2.69 \pm 0.10	296.44 \pm 2.49	0.69
		VU108-Z8b_1		2.67 \pm 0.01	1.50	65.57	7/11	17.25	0.11 \pm 0.04	2.55 \pm 0.05	301.53 \pm 1.14	0.71
		Combined (Z8)		2.66 \pm 0.01	2.51	67.27	22/35	16.87	0.14 \pm 0.02	2.61 \pm 0.05	300.01 \pm 1.18	2.78
Korokia dome	G15M0 029 ^d	VU108-Z16a		2.67 \pm 0.01	0.96	23.61	4/13	56.34	0.53 \pm 0.05	2.68 \pm 0.02	296.64 \pm 3.18	1.25
		VU108-Z16b_1	36.7465 N 24.5200 E	2.69 \pm 0.01	1.32	27.08	3/13	55.78	0.55 \pm 0.04	2.67 \pm 0.03	301.16 \pm 4.72	2.13
		Combined (Z16)		2.68 \pm 0.01	1.66	25.30	7/26	56.10	0.54 \pm 0.03	2.67 \pm 0.02	300.00 \pm 2.94	1.98
Coherent dacite of Profitis Ilias volcano	G15M0 015 ^c	VU108-Z9a		3.12 \pm 0.02	9.07	43.07	3/12	42.73	1.31 \pm 0.05	3.06 \pm 0.02	304.19 \pm 1.25	0.01
		VU108-Z9b_1	36.6629 N 24.3596 E	2.98 \pm 0.02	4.53	27.00	4/14	39.35	0.98 \pm 0.06	3.04 \pm 0.02	293.83 \pm 1.38	1.14
		Combined (Z9)		2.99 \pm 0.02	5.54	22.79	6/26	41.77	1.00 \pm 0.04	3.06 \pm 0.02	292.77 \pm 1.62	1.90
Coherent dacite of Profitis Ilias volcano	G15M0 017 ^c	VU108-Z7a		3.64 \pm 0.08	3.13	28.62	7/13	9.77	1.04 \pm 0.02	4.14 \pm 0.49	293.87 \pm 4.77	3.44
		VU108-Z7a_4	36.6596 N 24.3675 E	4.10 \pm 0.06	2.13	34.71	6/17	9.08	1.10 \pm 0.01	4.11 \pm 1.40	298.44 \pm 15.51	3.24
		VU108-Z7b_1		3.41 \pm 0.05	3.95	31.41	5/13	9.95	1.00 \pm 0.03	3.68 \pm 0.71	295.97 \pm 7.34	7.09
		Combined (Z7)		3.63 \pm 0.08	14.04	31.40	18/43	9.59	1.04 \pm 0.02	2.19 \pm 0.32	311.31 \pm 3.60	10.19

The age in bold is considered as the best estimate of the eruptive age.

The $^{40}\text{Ar}^*$ (%) is the average radiogenic ^{40}Ar of the analyses included in the weighted mean.

The experiment was analyzed on biotite^b, obsidian^d, amphibole^a and groundmass^c of a sample.

The same steps were used for the calculation of isochron ages as used in the weighted mean ages.

Table 3. $^{40}\text{Ar}/^{39}\text{Ar}$ results of single grain fusion analyses on the Milos volcanic field.

Volcanic unit	Sample-ID	Irr-ID	Location	Age $\pm 1\sigma$ (Ma)	MS WD	$^{39}\text{Ar}_K$ (%)	n/ntotal	$^{40}\text{Ar}^*$ (%)	K/Ca $\pm 1\sigma$	Inverse isochron age (Ma)	$^{40}\text{Ar}/^{36}\text{Ar} \pm 1\sigma$	MS WD
Fyriplaka complex	G15M0008 ^B	VU110-Z22	36.6729 N 24.4670 E	0.71 \pm 0.06	0.41	25.78	8/23	8.67	17.5 \pm 1.8	0.64 \pm 0.20	302.75 \pm 12.62	0.46
	G15M0012 ^B	VU110-Z24	36.6795 N 24.4828 E	1.12 \pm 0.11	2.26	60.49	14/23	7.32	14.9 \pm 0.8	0.26 \pm 0.07	316.75 \pm 19.49	2.29
	G15M0009 ^B	VU110-Z23	36.6716 N 24.4891 E	0.65 \pm 0.07	1.16	79.91	19/23	5.87	12.0 \pm 0.5	0.28 \pm 0.07	309.57 \pm 16.01	1.22
Trachilas complex	G15M0007 ^B	VU110-Z12	36.7671 N 24.4124 E	0.47 \pm 0.05	0.75	72.65	15/22	9.09	14.8 \pm 0.5	0.55 \pm 0.12	293.95 \pm 11.30	0.80
Kalamos lava	G15M0033 ^B	VU108-Z19	36.6662 N 24.4652 E	0.412 \pm 0.004	1.10	77.24	8/10	22.22	20.5 \pm 2.7	0.39 \pm 0.02	303.32 \pm 3.06	0.89
Trachilas complex	G15M0034 ^B	VU108-Z20	36.7550 N 24.4244 E	0.51 \pm 0.02	0.95	56.92	6/10	3.53	13.7 \pm 1.2	0.61 \pm 0.08	296.45 \pm 1.65	0.92
	G15M0035 ^B	VU108-Z21	36.7550 N 24.4244 E	0.63 \pm 0.02	1.26	73.43	6/9	4.87	17.7 \pm 1.1	0.77 \pm 0.13	294.99 \pm 3.17	1.42
Halepa lava dome	G15M0013 ^B	VU108-Z13	36.6716 N 24.4406 E	1.04 \pm 0.01	1.62	82.40	9/10	26.30	*15.2 \pm 0.2	1.02 \pm 0.04	299.77 \pm 4.06	0.00
Triades lava dome	G15M0021 ^B	VU110-Z4	36.7402 N 24.3397 E	2.48 \pm 0.04	1.49	87.08	4/12	36.09	13.00 \pm 0.60	3.44 \pm 0.46	228.58 \pm 36.66	1.39
	G15M0022 ^B	VU108-Z14	36.7402 N 24.3397 E	2.10 \pm 0.01	1.37	100.00	10/10	36.04	*11.7 \pm 0.2	2.08 \pm 0.06	299.44 \pm 4.63	1.59
	G15M0023 ^B	VU108-Z3	36.7263 N 24.3420 E	2.10 \pm 0.01	1.72	55.58	6/11	35.93	*76.1 \pm 2.4	2.13 \pm 0.06	296.12 \pm 4.63	2.08
	G15M0024 ^B	VU108-Z15	36.7277 N 24.3415 E	2.13 \pm 0.01	0.46	63.67	6/10	29.74	22.5 \pm 3.2	2.09 \pm 0.03	300.50 \pm 1.58	0.23
Mavros Kavos lava dome	G15M0025 ^B	VU108-Z2	36.6876 N 24.3515 E	2.36 \pm 0.01	0.70	84.62	9/10	37.62	43.2 \pm 2.7	2.34 \pm 0.04	300.57 \pm 3.49	0.78
	G15M0026 ^B	VU108-Z1b	36.6848 N 24.3500 E	2.35 \pm 0.01	1.36	95.23	9/10	38.56	12.8 \pm 2.3	2.42 \pm 0.04	292.01 \pm 2.92	0.93
Kalegeros crypto-dome	G15M0006 ^B	VU108-Z11	36.7643 N 24.5157 E	2.72 \pm 0.01	1.95	87.67	9/10	47.90	*28.3 \pm 0.5	2.62 \pm 0.04	310.21 \pm 4.04	0.99

The age in bold is considered as the best estimate of the eruptive age.

The $^{40}\text{Ar}^*$ (%) is the average radiogenic ^{40}Ar of the analyses included in the weighted mean.

*The K/Ca ratio is calibrated by removing the total fusion with excess ^{37}Ar (Ca) (fA>1).

^BThe experiment was analyzed on biotite of the sample.

The same steps were used for the calculation of isochron ages as used in the weighted mean ages.

Table 4. Major-element composition of volcanic samples from the Milos Volcanic Field.

Sample-ID	G15M0 008	G15M0 012	G15M0 009	G15M0 007	G15M0 033	G15M0 034	G15M0 035	G15M0 013	G15M 0020	G15M 0019	G15M00 32B	G15M0 004
Rock Types	Pumice	Pumice	Pumice	Pumice	Pumice	Pumice	Pumice	Rhyolite	-	Dacite	Obsidian	Dacite
Period	III							II				
Major elements (wt.%)												
SiO ₂	76.71	75.47	76.02	76.68	76.68	76.89	78.40	72.87	-	64.26	75.57	63.56
TiO ₂	0.14	0.13	0.13	0.08	0.10	0.08	0.08	0.22	-	0.56	0.20	0.57
Al ₂ O ₃	12.96	12.77	12.91	12.60	12.86	12.64	12.93	14.11	-	16.08	13.32	16.09
Fe ₂ O ₃	1.11	1.08	1.04	0.85	0.88	0.84	0.85	1.95	-	5.33	1.46	5.70
MnO	0.06	0.06	0.06	0.08	0.09	0.09	0.09	0.07	-	0.11	0.06	0.11
MgO	0.22	0.22	0.23	0.11	0.18	0.11	0.11	0.51	-	2.42	0.33	2.81
CaO	1.27	1.27	1.19	0.75	0.85	0.74	0.76	2.23	-	5.33	1.71	6.01
Na ₂ O	4.04	4.12	3.99	3.58	3.71	3.50	3.49	3.73	-	3.60	3.95	3.49
K ₂ O	3.22	3.15	3.41	4.74	4.46	4.85	4.95	3.43	-	1.69	3.26	1.57
P ₂ O ₅	0.02	0.02	0.02	0.01	0.01	0.01	0.01	0.04	-	0.04	0.03	0.09
BaO	0.06	0.06	0.06	0.05	0.05	0.05	0.05	0.06	-	0.04	0.06	0.04
L.O.I.	0.16	0.35	0.16	0.17	0.14	0.33	0.06	0.13	-	0.09	0.07	0.04
Total	99.97	98.70	99.22	99.70	100.01	100.13	101.78	99.35	-	99.55	100.02	100.08

Commented [JM35]: add information on the unit the sample belongs to

Sample-ID	G15M0 021	G15M0 022	G15M0 023	G15M0 024	G15M0 025	G15M0 026	G15M0 006	G15M0 016	G15M0 029	G15M0 015	G15M0 017
Rock Types	Trachy- dacite	Enclave	Dacite	Rhyolite	Dacite	Dacite	Dacite	Basaltic Andesite	Dacite	Dacite	Dacite
Period	II				I						
Major elements (wt.%)											
SiO ₂	64.98	53.87	73.05	76.57	69.56	69.57	68.58	55.72	61.91	63.77	68.03
TiO ₂	0.35	0.60	0.29	0.23	0.42	0.43	0.40	0.66	0.79	0.64	0.58
Al ₂ O ₃	16.82	19.91	14.24	11.73	15.30	16.08	15.90	18.43	17.09	16.33	15.90
Fe ₂ O ₃	3.69	7.61	3.23	1.69	3.15	3.38	2.67	7.70	5.90	5.42	3.47
MnO	0.08	0.16	0.02	0.03	0.11	0.04	0.07	0.14	0.09	0.10	0.07
MgO	1.50	3.93	0.53	0.46	0.88	0.62	0.81	4.42	1.84	2.48	1.34
CaO	2.19	5.45	2.35	2.36	3.67	3.43	2.89	8.78	6.07	5.91	4.31
Na ₂ O	2.61	1.73	3.28	2.85	3.49	3.56	4.19	2.90	3.57	3.35	3.76
K ₂ O	7.24	6.11	3.36	2.31	2.98	2.63	3.61	1.41	2.71	1.91	2.69
P ₂ O ₅	0.05	0.08	0.04	0.05	0.11	0.09	0.11	0.09	0.20	0.09	0.10
BaO	0.35	0.34	0.06	0.05	0.06	0.06	0.10	0.03	0.13	0.04	0.04
L.O.I.	0.17	0.21	0.12	0.20	0.19	0.09	0.12	0.06	0.09	0.04	0.48
Total	100.03	100.00	100.57	98.53	99.92	99.98	99.45	100.34	100.39	100.08	100.77

The classification of rock type for each sample is on the basis of field observation and SiO₂ versus K₂O plot of Le Bas et al. (1986). All iron expressed as Fe₂O₃(total).

Table 5. Summary of the eruption ages of the Milos volcanic field

No.	Name of volcanic centre	Age (Ma)	Reference
1	Kimlos volcano	3.34	Fytikas et al., 1986
2	Profitis Iliias crypto/pumice cone	3.08	Fytikas et al., 1986
3	coherent dacite of Profitis Iliias volcano	3.06	This study
4	Filakopi volcano	2.66	Stewart and McPhie, 2006
5	Kalegeros cryptodome	2.62	This study
6	Mavro Vouini lava dome	2.5	Angelier et al., 1977
7	Mavros Kavos lava dome	2.42-2.36	This study
8	Polyegos lava dome	2.34	Fytikas et al., 1986
9	Triades lava dome	2.13-2.10 and 1.97	This study
10	Adamas lava dome	2.03	Fytikas et al., 1986
11	Dhemeneghaki volcano	1.83	This study
12	Bombardo volcano	1.71	Fytikas et al., 1986
13	Korakia dome	1.59	Fytikas et al., 1986
14	Komntaro dome	1.52-1.48	This study
15	Halepa lava dome	1.04	This study
16	Plakes lava dome	0.97	Fytikas et al., 1986
17	Trachilias complex	0.63, 0.51 and 0.317	This study
18	Kalamos lava dome	0.41	This study
19	Antimilos domes	0.32	Fytikas et al., 1986
20	Fyriplaka complex	0.11 and 0.07-0.06	This study
21	Phreatic activity	200 AD-200 BC	Trainau and Dalabakis, 1989

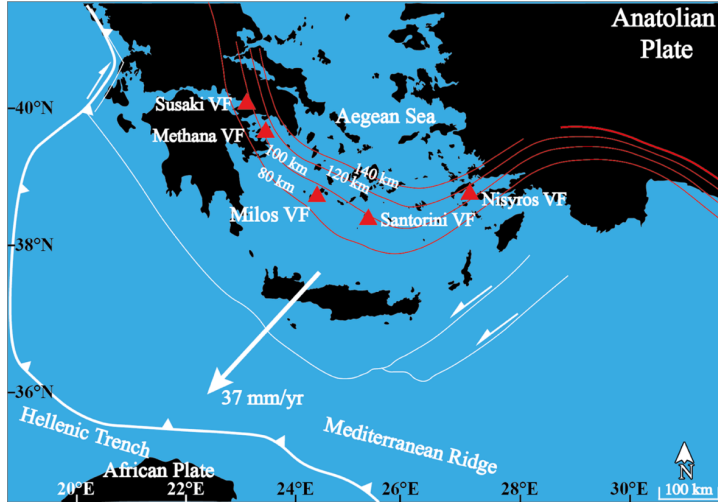


Figure 1. Map of the South Aegean Volcanic Arc (SAVA). Volcanic fields (VF) are indicated by red triangles: Susaki, Methana and Milos VFs in the western SAVA, Santorini VF in the centre and Nisyros VF in the eastern SAVA. Red contour lines show the depth to the Benioff zone (Hayes et al., 2018). White arrow represents the GPS-determined plate velocity of the Aegean microplate relative to the African plate from Doglioni et al. (2002).

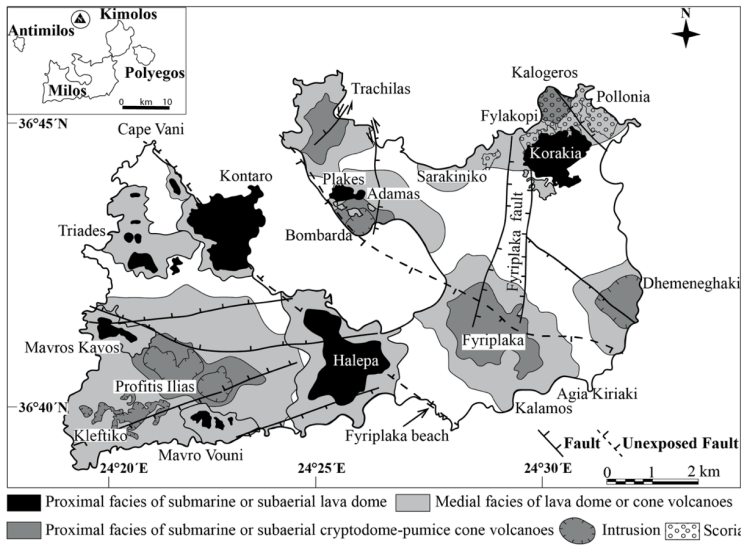


Figure 2. Distribution of the proximal and medial facies of the submarine pumice cone/crypto dome volcanoes, submarine, submarine-subaerial and subaerial domes and rhyolitic complexes (tuff cone and associated lava) of Milos, modified after Fytikas et al. (1986) and Stewart and McPhie (2006). The distal facies of Stewart and McPhie (2006) is not shown.

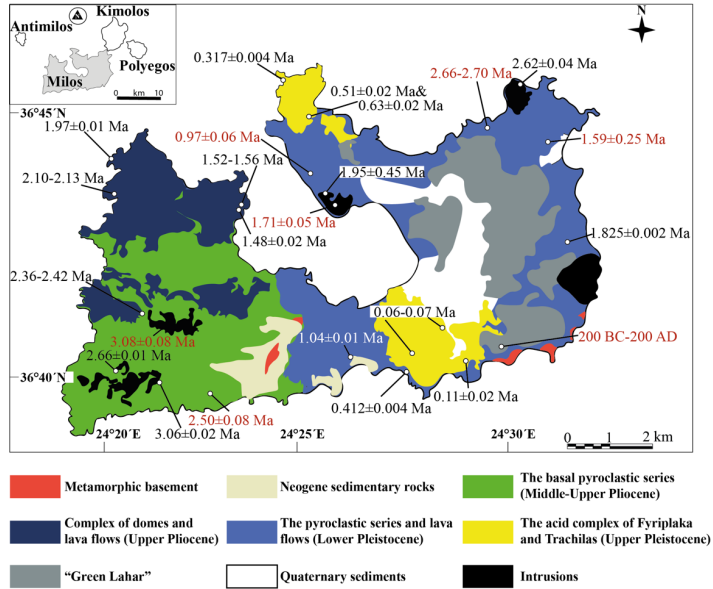


Figure 3. Simplified geological map of Milos with our $^{40}\text{Ar}/^{39}\text{Ar}$ ages and sample locations of key volcanic deposits, modified after Stewart and McPhie (2006) and Grasemann et al. (2018). The stratigraphic units of Milos are from Fytikas et al. (1986). Age data from this study are in black, published ages are shown in red (Angelier et al., 1977, Fytikas et al., 1986, Traineau and Dalabakis, 1989, and Stewart and McPhie, 2006). The "Green Lahar" (Fytikas, 1977) consists of deposits from multiple phreatic explosions and contains fragments of metamorphic, sedimentary and volcanic rocks.

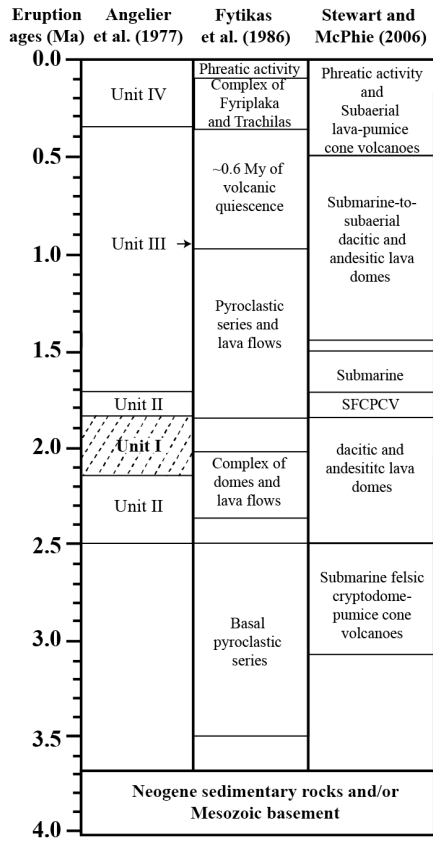


Figure 4. Previous proposed stratigraphic frameworks for Milos by Angelier et al. (1977), Fytikas et al. (1986) and Stewart and McPhie (2006). Volcanic unit II of Angelier et al. (1977) contains unit I. Stewart and McPhie (2006) described the volcanic faces of Milos mainly based on the geochronological works of Angelier et al. (1977) and Fytikas et al. (1986). Abbreviation: SFCPCV=Submarine felsic cryptodome-pumice cone volcanoes.

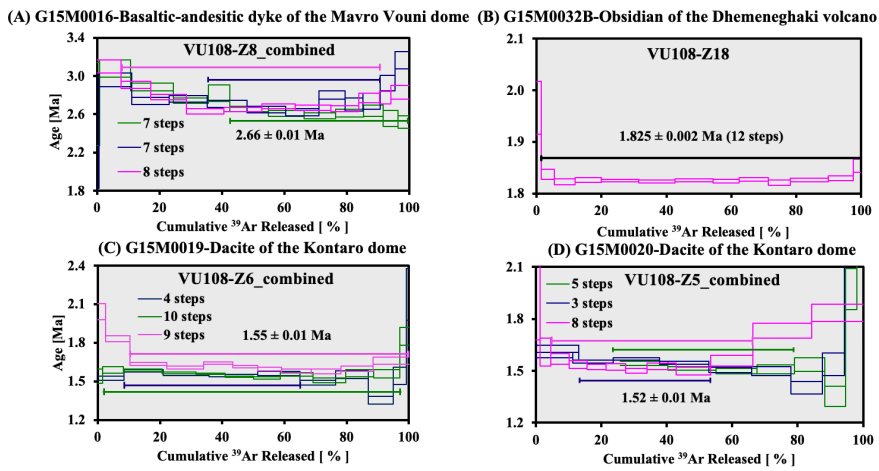


Figure 5. Groundmass $^{40}\text{Ar}/^{39}\text{Ar}$ plateau ages for samples G15M0016 (A), G15M0032B (B), G15M0019 (C) and G15M0020 (D). The Mavro Vouni dome (A), Dhemenehaki volcano (B) and Kontaro dacitic dome (C, D) are located in respectively the south-western, north-eastern and eastern parts of Milos VF (see Fig. 2). Final age calculation is reported with 1σ errors. See the individual steps of sample G15M0016, G15M0019 and G15M0029 in supplementary material II.

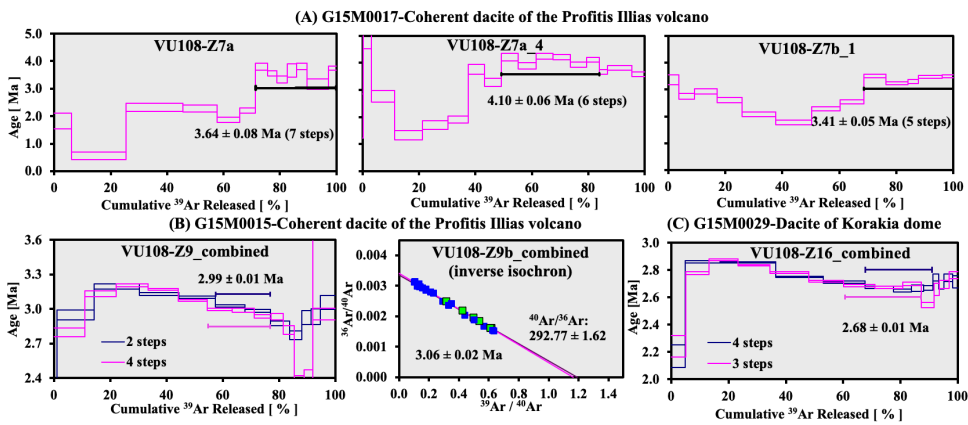


Figure 6. Groundmass $^{40}\text{Ar}/^{39}\text{Ar}$ plateau or inverse isochron ages for samples G15M0017 (A), G15M0015 (B) and G15M0029 (C). Individual steps and final age calculation are reported with 1σ errors. The Profitis Ilias volcano (A, B) and dacitic Korakia dome (C) are located in the south-western and north-eastern parts of Milos VF, respectively (see Fig. 2). See the individual steps of sample G15M0015 and G15M0029 in supplementary material II.

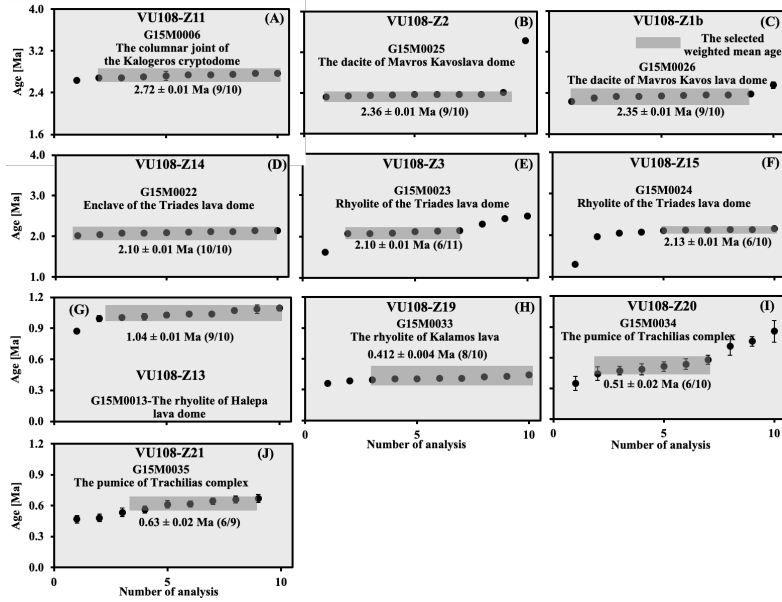


Figure 7. Biotite $^{40}\text{Ar}/^{39}\text{Ar}$ total fusion ages for samples G15M0006 (A) and G15M0025-26(B, C), G15M0022-24 (D-F), G15M0013 (G) and G15M0033-35 (H-J). Data outside shaded area are not included in the weighted mean. Individual steps and final age calculation are reported with 1σ errors. The Kalogeros cryptodome and Mavros Kavos lava dome are located in the north-eastern and south-western parts of Milos VF, respectively, and Triades lava dome, Halepa lava dome, Trachilias complex and the Kalamos lava are situated in the southern, northern and south-eastern parts of Milos VF, respectively (see Fig. 2).

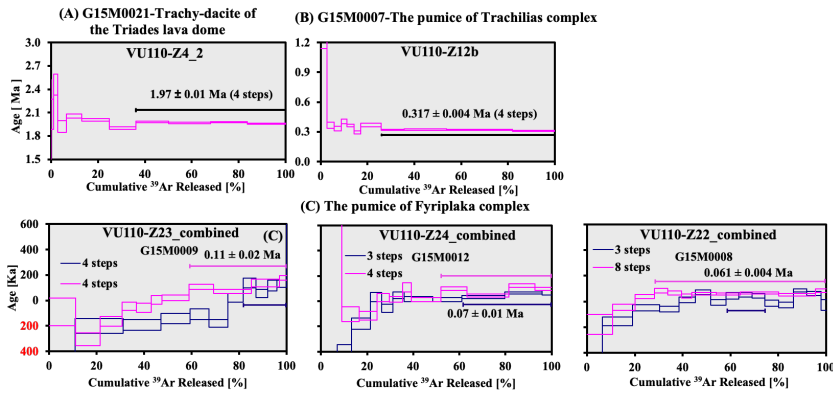


Figure 8. Biotite $^{40}\text{Ar}/^{39}\text{Ar}$ plateau ages for samples G15M0021 (A), G15M0007 (B), and G15M0009 (VU110-Z23_combined), G15M0012 (VU110-Z24_combined) and G15M0008 (VU110-Z22_combined) (C). The numbers in red represent negative ages. Individual steps and final age calculation are reported with 1σ errors. The Triades lava dome, Trachilias and Fyriplaka complexes are located in the north-western, northern and south-eastern parts of Milos VF, respectively (see Fig. 2). See the individual steps of sample G15M0021, G15M0007, G15M0009, G15M0012 and G15M0008 in supplementary material II.

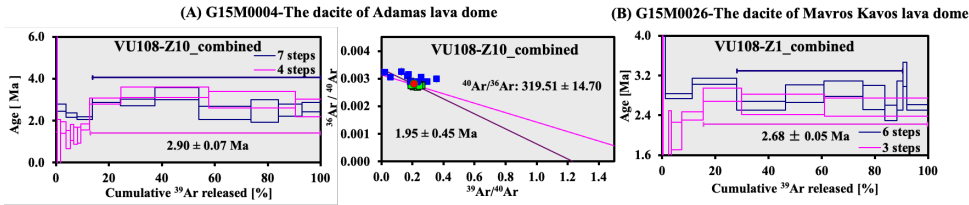


Figure 9. Amphibole $^{40}\text{Ar}/^{39}\text{Ar}$ plateau or inverse isochron ages for samples G15M0004 (A) and G15M0026 (B). Final age calculation is reported with 1σ errors. The Adamas and Mavros Kavos lava domes are located in the northern and south-western parts of Milos VF, respectively (see Fig. 2). See the individual steps of sample G15M0004 and G15M0026 in in supplementary material II.

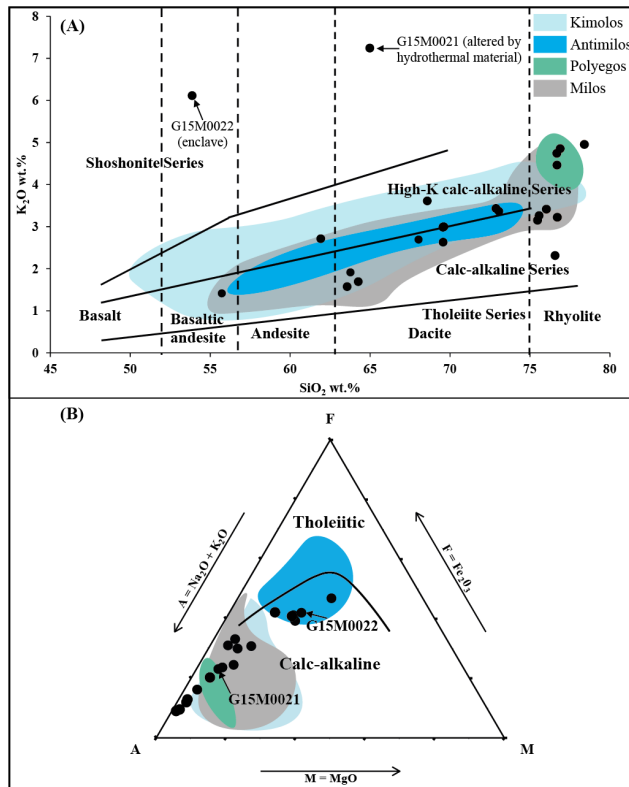
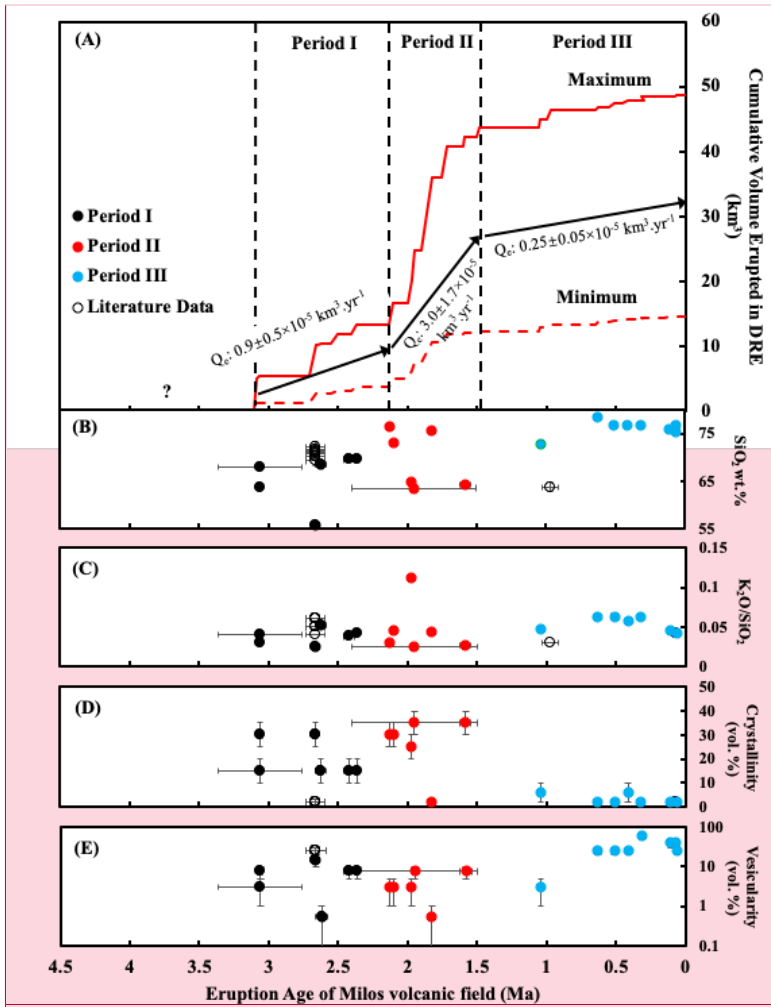


Figure 10. SiO₂ versus K₂O (A) and AFM (B) diagrams for the Milos volcanic field with data of this study as solid circles. Published data are represented by shaded fields (Francalanci and Zelmer, 2019 and reference therein). Fields for the tholeiitic, calc-alkaline, high-K calc-alkaline and shoshonitic series are from Peccerillo and Taylor (1976). Vertical lines defining fields for basalt, basaltic-andesite, andesite, dacite and rhyolite are from Le Bas et al. (1986). The solid line dividing tholeiitic and calc-alkaline fields is from Irvine and Baragar (1971).



Commented [JM36]: The only data you can rely on are the ages and the compositions. Delete the crystallinity and vesicularity plots entirely

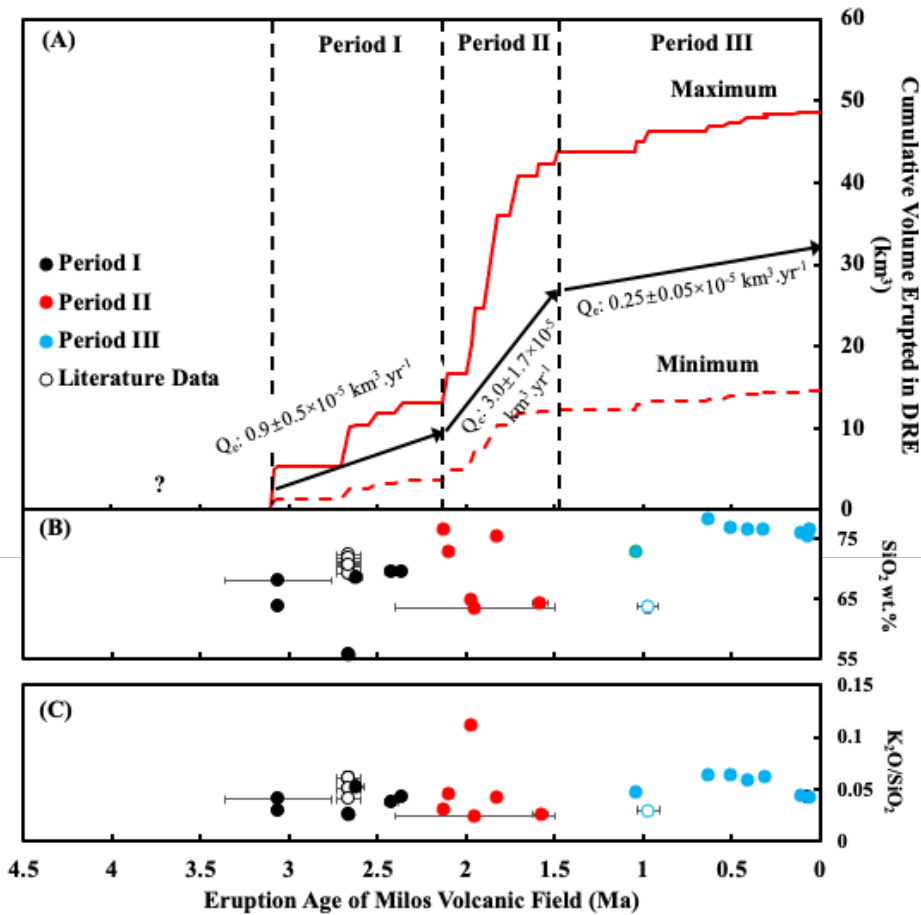


Figure 11. Eruption age versus (A) cumulative eruption volume for the volcanic deposits of Milos, (B) SiO_2 wt.%, (C) $\text{K}_2\text{O}/\text{SiO}_2$, (D) crystallinity vol.% and (E) vesicularity vol.% of Milos volcanic units of this study and previous studies. The maximum (Max; red line) and minimum (Min; dashed red line) cumulative eruption volume curves were estimated from Campos et al. (1996) and Stewart and McPhie (2006). Q_v is the long-term volumetric volcanic output rate (see discussion). The exact volume of volcanic products between 4.1 and 3.08 Ma is not well constrained and indicated with a question mark. In this study, the estimations of crystallinity and vesicularity on the older samples (>1.0 Ma) are all from lava and domes. Most of the younger samples (<1.0 Ma) are pumiceous pyroclastic units. The major element, crystallinity and vesicularity data of the old pumices of Filakopi volcanoes (2.66 Ma) are from Stewart (2003). The major element data of the Plakes lava dome is from Fytikas et al. (1986). Geochemical, crystallinity and vesicularity data of the old pumices of the Profitis Ilias (~ 3.08 Ma) is lacking due to the severe alteration.

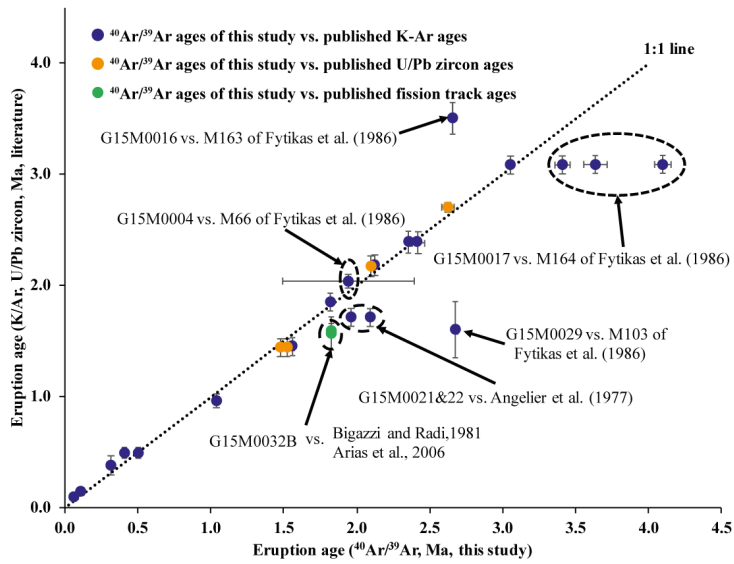


Figure 12. The $^{40}\text{Ar}/^{39}\text{Ar}$ ages of this study (x-axis) compared to the K/Ar ages (Angelier et al., 1977; Fytikas et al., 1986), U/Pb zircon ages (Stewart and McPhie, 2006) and fission track ages (Bigazzi and Radi, 1981; Arias et al., 2006) (y-axis) for the same volcanic units. Ages which deviate from the 1:1 correlation line are discussed in section 4.1.

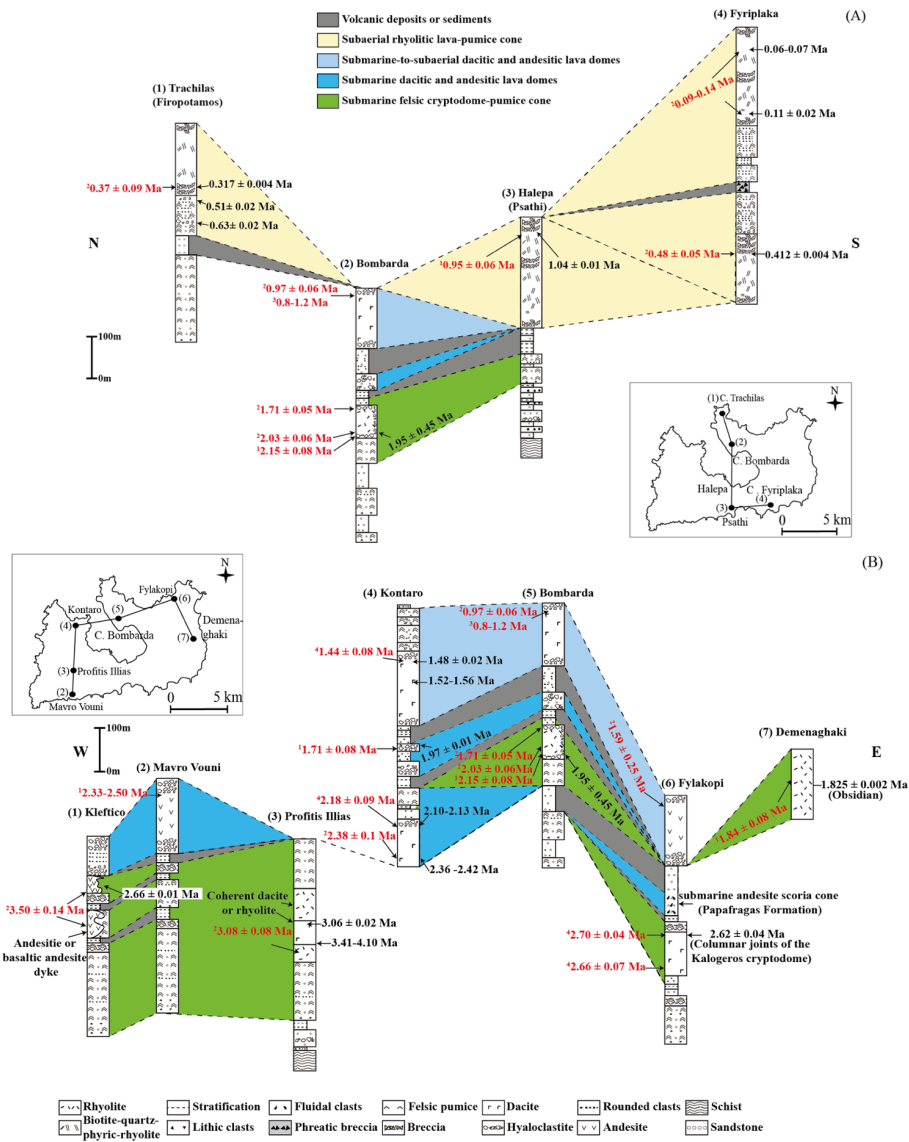


Figure 14.13. Nine selected stratigraphic columns covering the (A) young (<1.4 Ma) and (B) old (>1.4 Ma) volcanic deposits of Milos modified after Stewart and McPhie (2006), except for (7) Demenaghaki. Age data in black are from this study and in red are from: 1=Angelier et al. (1977), 2=Fytikas et al. (1976, 1986), 3=Matsuda et al. (1999), 4=Stewart and McPhie (2006).

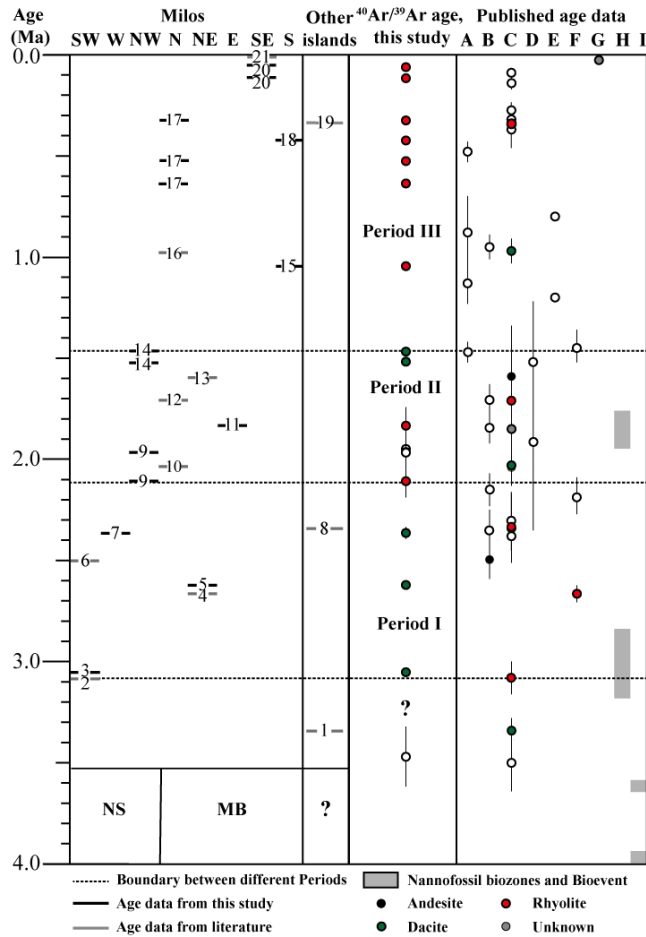


Figure 14. Diagram presenting three periods of different ~~long-term~~ volumetric volcanic output rate on Milos volcanic field based on the new $^{40}\text{Ar}/^{39}\text{Ar}$ Ar data of this study and published data. The location of the different volcanoes is given in Fig 2 and indicated in the left panel (from left to right: SW, W, NW, N, NE, E, SE and S of Milos). The right panel corresponds to published age data: [A]=Fytikas et al., 1976, [B]=Angelier et al., 1977, [C]=Fytikas et al., 1986, [D]= Bigazzi & Radi, 1981, [E]=Matsuda, 1999, [F]=Stewart and McPhie (2006), [G]= Trainau and Dalabakis, 1989, and Biostratigraphic data of the Neogene sediments (NG) is from [H]=Calvo et al. (2012) and [I]=Van Hinsbergen et al. (2004) calibrated to Raffi et al. (2020) (LCO of *Sphenolithus* spp. and FO of *D. tamalis*). The number in the left panel represents the volcanic centres of Milos (see details in Table 5). The start of volcanism (3.08-3.61 Ma) on Milos and the basement of the other Islands (Antimilos, Kimolos and Polyegos) are not well constrained and indicated with question marks (see text for discussion). The simplified basement cross-section (NS: Neogene sedimentary rock; MB: Metamorphic basement) under Milos volcanic units is based on Fytikas et al. (1989). We used the filled symbols as the best estimate for the eruption ages at the different volcanic centres, and the open symbols are not used as the best estimate due to their relatively large uncertainties.

Commented [JM37]: what do open symbols mean?